



Axon guidance at the spinal cord midline—A live imaging perspective

Alexandre Dumoulin^{1,2}  | Nikole R. Zuñiga^{1,2}  | Esther T. Stoeckli^{1,2} 

¹Department of Molecular Life Sciences, University of Zurich, Zurich, Switzerland

²Neuroscience Center Zurich, University of Zurich, Zurich, Switzerland

Correspondence

Esther T. Stoeckli, Department of Molecular Life Sciences, University of Zurich, Winterthurerstrasse 190, 8057 Zurich, Switzerland.
Email: esther.stoeckli@mls.uzh.ch

Funding information

Swiss National Science Foundation

Abstract

During neural circuit formation, axons navigate several choice points to reach their final target. At each one of these intermediate targets, growth cones need to switch responsiveness from attraction to repulsion in order to move on. Molecular mechanisms that allow for the precise timing of surface expression of a new set of receptors that support the switch in responsiveness are difficult to study in vivo. Mostly, mechanisms are inferred from the observation of snapshots of many different growth cones analyzed in different preparations of tissue harvested at distinct time points. However, to really understand the behavior of growth cones at choice points, a single growth cone should be followed arriving at and leaving the intermediate target. Existing ex vivo preparations, like cultures of an “open-book” preparation of the spinal cord have been successfully used to study floor plate entry and exit, but artifacts prevent the analysis of growth cone behavior at the floor plate exit site. Here, we describe a novel spinal cord preparation that allows for live imaging of individual axons during navigation in their intact environment. When comparing growth cone behavior in our ex vivo system with snapshots from in vivo navigation, we do not see any differences. The possibility to observe the dynamics of single growth cones navigating their intermediate target allows for measuring growth speed, changes in morphology, or aberrant behavior, like stalling and wrong turning. Moreover, observation of the intermediate target—the floor plate—revealed its active participation and interaction with commissural axons during midline crossing.

KEYWORDS

axon guidance, commissural neurons, floor plate, live imaging, midline, neural circuit formation, spinal cord culture

1 | INTRODUCTION

Commissural axons in the developing spinal cord have been used for over two decades to learn fundamental molecular mechanisms of axon guidance (Stoeckli, 2018). The dl1 subtype of dorsal commissural interneurons are an excellent model, as their axons have a

stereotypical trajectory at the ventral midline, as all axons of this subpopulation cross the floor plate (FP), exit it and turn rostrally along the contralateral border. Thus, dl1 commissural neurons offer an easy read-out for deciphering molecular mechanisms of axon guidance at choice points. Since the first application of lipophilic dye tracing in open-book preparations of rat spinal cords that revealed the normal

This is an open access article under the terms of the Creative Commons Attribution License, which permits use, distribution and reproduction in any medium, provided the original work is properly cited.

© 2021 The Authors. *The Journal of Comparative Neurology* published by Wiley Periodicals LLC.

trajectory of these axons 30 years ago (Bovolenta & Dodd, 1990), this method continues to be used to assess axon guidance at the midline in mouse and chicken embryos. The comparison between axons in open-book preparations of control and experimentally manipulated spinal cords, dissected at specific time points, offered a solid understanding of molecules involved in axonal midline crossing and subsequent turning in higher vertebrates. However, the information about mechanisms that can be extracted from such experiments is limited, as it is deduced from snapshots of axons taken from different animals sacrificed at a specific time point. For this reason, we have established a live-imaging approach that allows for visualization of dl1 axonal behavior at the FP, while axons are in the process of crossing the midline and then turning rostrally. We have chosen the chicken embryo, as it is a very accessible model for studying various developmental processes in intact tissues *in vivo* and *ex vivo* (Boubakar et al., 2017; Das & Storey, 2014; Li et al., 2019; Sanders et al., 2013). Thanks to a very stable and reproducible spinal cord culture, we could for the first time characterize the exact timing of midline crossing and the details of rostral turning by dl1 axons in an intact environment in control and experimentally manipulated spinal cords. We could get more insight into growth cone dynamics and morphologies at their choice point, the FP. Furthermore, our *ex vivo* method also shed new light on the role of the intermediate target, the FP cells, their dynamics, morphology and interaction with commissural axons during midline crossing. Finally, our results on the dynamic behavior of growth cones at the spinal cord midline allowed us to compare axonal behavior at different choice points, such as the optic chiasm, reported previously (Godement et al., 1994; Sretavan & Reichardt, 1993).

2 | MATERIALS AND METHODS

2.1 | *In ovo* electroporation

Plasmids encoding farnesylated td-Tomato under control of the Math1 enhancer and the β -globin promoter for dl1 neuron-specific expression (Math1::tdTomato-F, 700 ng/ μ l) and farnesylated EGFP under control of the β -actin promoter (β -actin::EGFP-F, 30 ng/ μ l) were coinjected into the central canal of the chicken neural tube *in ovo* at HH17-18 (Hamburger & Hamilton, 1951) and unilaterally electroporated, using a BTX ECM830 square-wave electroporator (five pulses at 25 V with 50 ms duration each), as previously described (Wilson & Stoeckli, 2012). A final concentration of 0.1% (vol/vol) of Fast Green was added to the plasmid mix to trace injection site and volume of the plasmid mix. After electroporation, embryos were covered with sterile PBS and eggs were sealed with tape and incubated at 39°C for 26–30 h, until embryos reached stage HH22, or for 36–46 h, until embryos reached HH24. For the FP study EGFP-F was expressed from a plasmid with the Hoxa1 enhancer and the β -globin minimal promoter (Wilson & Stoeckli, 2011) (Hoxa1::EGFP-F, 1000 ng/ μ l) and coinjected with the Math1::tdTomato-F plasmid (700 ng/ μ l) and unilaterally electroporated as above, or bilaterally

electroporated (three pulses in each direction at 25 V with 50 ms duration each). For knockdown of Fzd3 (or luciferase as control) in dl1 neurons (Math1 enhancer) plasmids previously published (Math1::EGFP-F; miFzd3 and Math1::EGFP-F; mi2Luc, 700 ng/ μ l) were coinjected with the β -actin::mRFP plasmid (30 ng/ μ l) and unilaterally electroporated at HH16 for more efficient knockdown (Alther et al., 2016).

2.2 | Dissection of intact spinal cords

Intact spinal cords were dissected from HH22 embryos in ice-cold, sterile PBS (Gibco) in a silicon-coated Petri dish with sterile instruments. Embryos were pinned down with their dorsal side down with thin needles (insect pins). Here, special care was taken not to damage or detach meninges surrounding the spinal cord by avoiding too much rostro-caudal and lateral tension. Internal organs and ventral vertebrae were removed to access the spinal cord. Ventral roots were cut off and the spinal cord was carefully extracted from the embryo with forceps, avoiding any excessive bending. Note that dorsal root ganglia were not cut off and all were still attached to the spinal cord. The ventral and dorsal midlines were kept intact throughout dissection. Finally, remaining dorsal tissues were discarded. See Figure 1 for a detailed step-by-step protocol to successfully dissect intact HH22 spinal cords. Note that this procedure can also be applied to older embryos (at least HH24–25). Once intact spinal cords were dissected and cleaned from any remaining dorsal tissues, they were embedded with the ventral side down in a warm (39°C) 100- μ l drop of 0.5% low-melting agarose in a 35-mm Ibidi μ -dish with glass bottom (Ibidi, #81158) (Figure 2(d,e); Figure 1(g); 3.5% agarose (FMC) was prepared in water, spinal cord medium (MEM with Glutamax [Gibco] supplemented with 4 mg/ml Albumax [Gibco], 1 mM pyruvate [Sigma], 100 units/ml Penicillin and 100 μ g/ml Streptomycin [Gibco]) was added to get 0.5% final agarose concentration). Note that the spinal cord should be as straight as possible with the dorso-ventral axis perpendicular to the glass bottom, as any pronounced curvature or tilting of the midline would induce axon guidance artifacts or death of the axons, respectively. To this end, a 12-mm flexiPERM conA ring (Sarstedt) was placed in the center of the culture dish before the agarose drop was added (the drop should not touch the ring). Hence, the medium added to the drop of low-melting agarose could touch the ring all around and therefore stabilize the position of the agarose drop and avoid any movement of the spinal cord during recordings thanks to surface tension (Figure 1(g)). Once the agarose solidified (around 5 min at room temperature), 200 μ l of spinal cord medium were added to the drop and the culture could be started.

2.3 | Dissection of open-books

Open-book preparations of spinal cords were dissected from HH24 embryos as previously described in a video protocol for HH25–26 embryos (Wilson & Stoeckli, 2012). The first steps were identical to the protocol for intact spinal cord dissection given above (steps a,b in

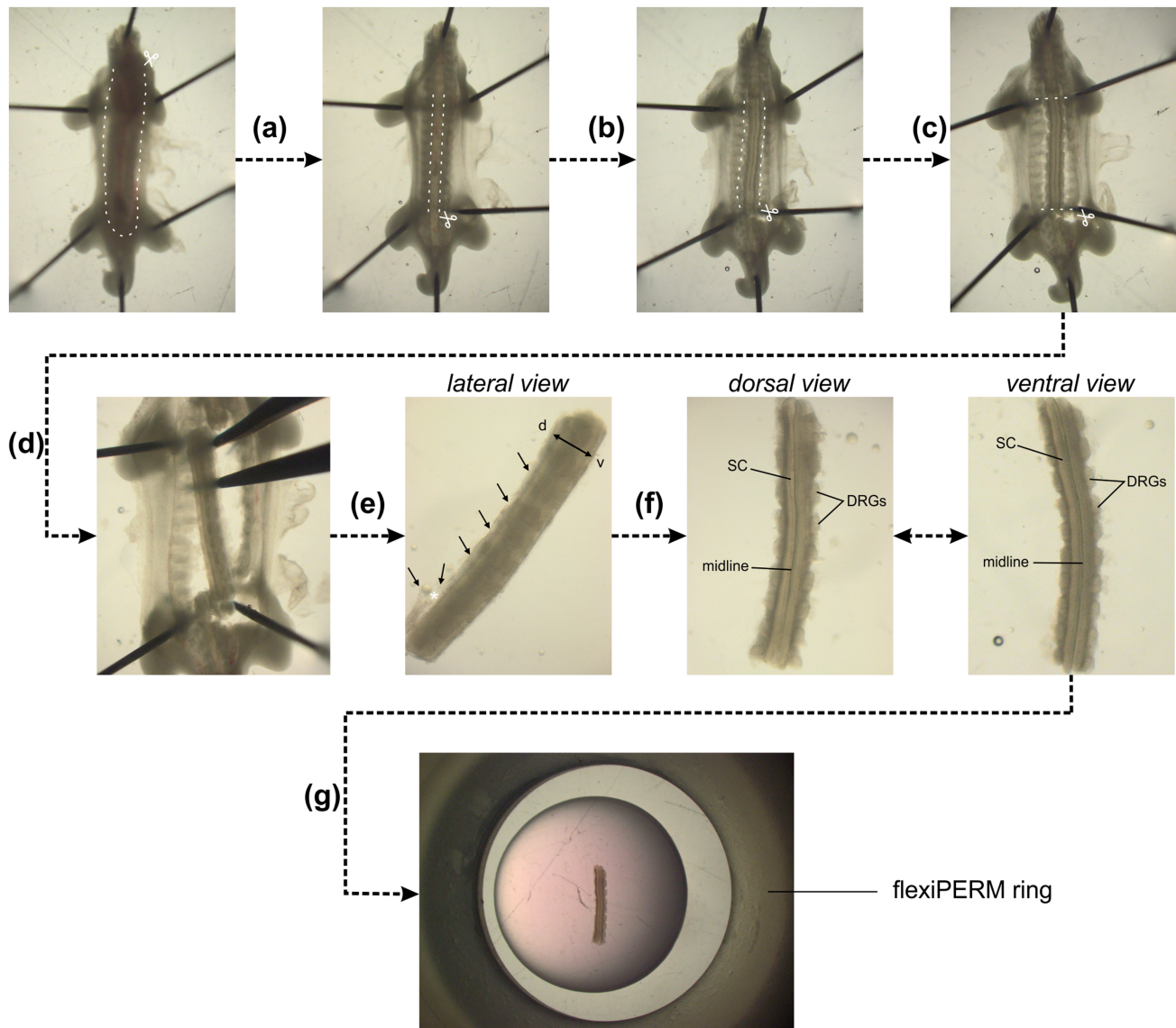


FIGURE 1 Dissection of intact spinal cords (SCs) from HH22 chicken embryos. (a) HH22 embryos were pinned down with the dorsal side down in a silicon-coated Petri dish in sterile, cold PBS. Internal organs were removed by first cutting the ventral skin along the dashed lines and pinching out the organs with forceps. (b) Then, a laminectomy was performed, that is, the ventral vertebrae were cut along the caudal–rostral axis at the level of the outer SC boundaries and the stripe of bone structure was removed with forceps. (c) The ventral roots exiting the ventral part of the SC and the peripheral processes of the dorsal root ganglia (DRG) were cut in parallel to the SC without cutting off any DRG. (d) The SC was then cut at the level of the wings and legs. (e) The SC with attached DRG was carefully separated from the rest of the embryo with forceps. Here, special care should be given not to bend the SC by stabilizing the tissue with a second forceps. (f) At this point, the dorsal skin and dermomyotome (black arrows) were removed by first inducing an opening with forceps (white asterisk) taking care not to damage the dorsal SC. Then, using forceps, the dorsal skin and dermomyotome were carefully removed all along the caudal–rostral axis. After this step, the dorsal SC should look as clean as the ventral SC with clearly visible midline and no remaining tissues attached (compare dorsal and ventral view). (g) Finally, the intact SC with attached DRG could be embedded as straight as possible in a drop of low-melting agarose-medium mix with the ventral side down. White dashed lines indicate where cuts with small spring scissors should be made

Figure 1). Starting there, the tension along the rostro-caudal axis was increased using the upper and lower needles and meninges were removed with a blade made of fire-polished tungsten wire. Spinal cords were cut transversally at the wing and leg levels and carefully extracted from the embryo with forceps. At this point, the dorsal midline spontaneously opened. Open-book preparations of spinal cords were then plated with the apical side down (Figure 2(g,h)) in the center of a 35-mm Ibidi μ -dish with glass bottom (Ibidi, #81158),

precoated with 20 μ g/ml poly-L-lysine (Sigma). A homemade, harp-like holder made out of a Teflon ring and thin nylon strings was used to keep the spinal cord in place (Figure 2(g)). Note that the strings were barely touching the open-books but stabilized the flat position of the spinal cord. Then, 100 μ l of 0.5% low-melting agarose (see above) were added on top of the spinal cord. Once the agarose solidified (around 5 min at room temperature), 200 μ l of spinal cord medium were added to the agarose drop and the culture could be started.

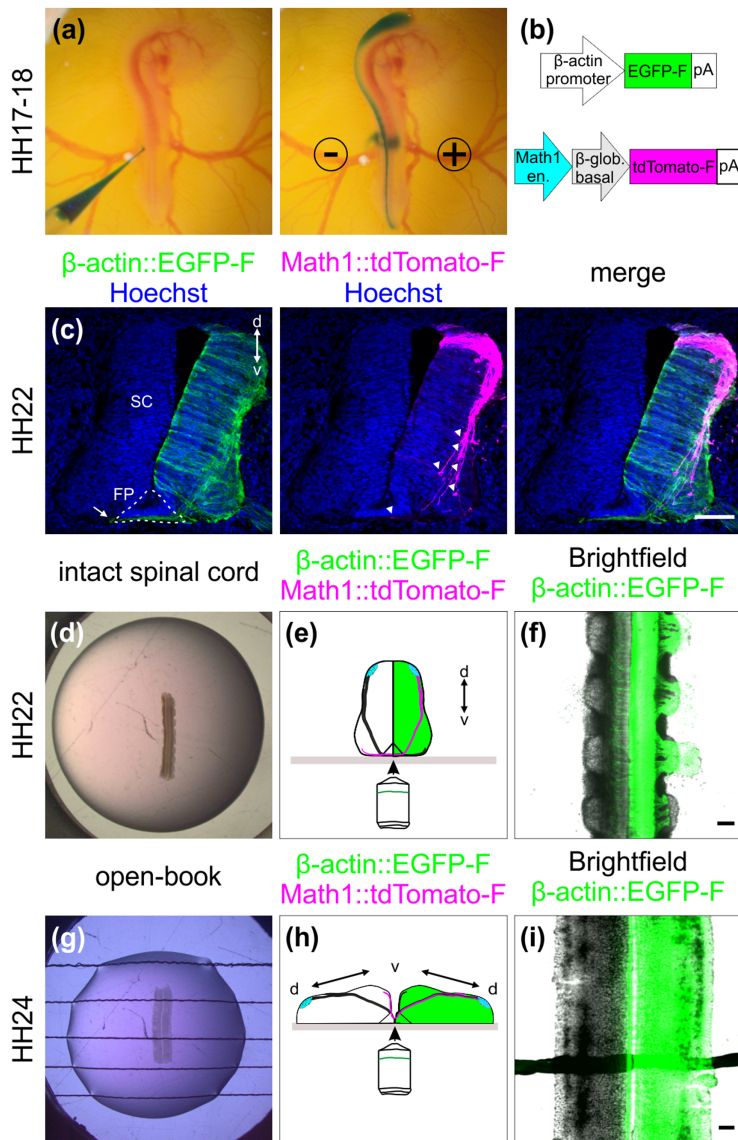


FIGURE 2 Labeling strategy for dl1 interneurons and spinal cord (SC) culture systems. (a–c) In ovo injection and electroporation of a plasmid mix to specifically label dl1 interneurons. (a) The plasmid mix was injected into the central canal of the SC of HH17-18 chicken embryo in ovo, followed by unilateral electroporation. (b) Plasmid constructs injected to target all cells (β -actin::EGFP-F) and dl1 interneurons (Math1::tdTomato-F). en., enhancer; β -glob., β -globin. (c) Immunostaining of a transverse cryosection of a HH22 SC taken from an embryo sacrificed 1 day after electroporation with the plasmids indicated in (b). At this stage, most dl1 growth cones were approaching the FP area, but none of them had crossed it yet (white arrowheads). However, a substantial number of Math1-negative, but EGFP-F-expressing commissural axons of more ventral populations had already crossed the FP at HH22 (arrow). (d–f) Intact SC culture. (d) Intact SCs of embryos injected and electroporated 1 day earlier were embedded with the ventral side down in a drop of low-melting agarose. (e) The ventral SC area was imaged with an inverted spinning disk microscope. The green-colored hemisphere represents the electroporated side of the SC. (f) Low magnification overview of a SC visualized with this set-up with cells expressing EGFP-F under the β -actin promoter on one side merged with the bright-field image. (g–i) Culture of an open-book preparation of a SC. (g) Intact open-book preparations of HH24 SCs dissected from embryos injected and electroporated about one and a half day earlier were embedded with the apical side down in an agarose drop with strings to hold it in place. (h) The midline area was visualized with the same inverted spinning disk microscope as above. The green-colored hemisphere represents the electroporated side of the SC. (i) Low magnification overview of a SC visualized with this set-up with cells expressing EGFP-F under the β -actin promoter on one side merged with the bright-field image. d, dorsal; v, ventral. Scale bars: 100 μ m

2.4 | Live imaging

Live imaging recordings were carried out with an Olympus IX83 inverted microscope equipped with a spinning disk unit (CSU-X1 10,000 rpm, Yokogawa). Cultured spinal cords were kept at 37°C with 5% CO₂ and 95% air in a PeCon cell vivo chamber (PeCon). Temperature and CO₂-levels were controlled by the cell vivo temperature controller and the CO₂ controller units (PeCon). Spinal cords were incubated for at least 30 min before imaging was started. We acquired 18–40 planes (1.5 μ m spacing) of 2 \times 2 binned z-stack images every 15 min for 24 h with a \times 20 air objective (UPLSAPO \times 20/0.75, Olympus) and an Orca-Flash 4.0 camera (Hamamatsu) with the Olympus CellSens Dimension 2.2 software. We performed most of our recordings in the lumbar level of the spinal cord and always took three channels of interest: emission at 488 and 561 nm, as well as bright field. Recordings of axons after Fzd3 or luciferase knockdown were performed at the thoracic level (see cartoon in Figure 5(g)). For higher magnification recordings, a \times 40 silicone oil objective was used (UPLSAPO S

\times 40/1.25, Olympus) with the same acquisition settings as above. Images taken every 5–15 min. The quantifications of growth cone behavior, such as splitting in the FP, formation of ventral–dorsal protrusions and protrusions before FP exit, were based on a time resolution of one stack taken every 15 min. The analysis of protrusions before FP exit could be done only on the first axons exiting the FP, because with time it was difficult to visualize the small protrusions correctly due to the increase in the density of axons at the FP exit site.

2.5 | Data processing and virtual tracing

Z-stacks and maximum projections of Z-stack movies were evaluated and processed using Fiji/ImageJ (Schindelin et al., 2012). The MtrackJ plugin (Meijering et al., 2012) was used to virtually trace single Math1-positive dl1 commissural axons crossing the FP. This helped to keep track of which axons had already been quantified. The leading edge (and not filopodia) of growth cones was always selected for each

time point. At the exit site, the central domain of the growth cone was selected with the tracing tool, as growth cones very often slightly changed their directionality and drastically change their shape before turning. For comparable analyses of axonal behavior and speed in the two halves of the FP, we only traced and quantified axons that entered, crossed and exited the FP during the 24-hour imaging period. Axons already in the FP at the beginning of the imaging period were not considered. Overlays of labeled axons with EGFP-F and bright-field channels were used to assess the FP boundaries and midline localization. The virtual tracing tool was also used to extract the local growth speed for each single axon. Local speed is defined here as the average speed calculated for the last 15 min time period. Note that the montage of dl1 commissural axons shown in Movie 2 was generated from z-stacks that were 2D deconvolved (nearest neighbor) using the Olympus CellSens Dimension 2.2 software and assembled with Fiji/ImageJ. All data acquired with higher magnification ($\times 40$ silicone oil objective) were 3D deconvolved using constrained iterative deconvolution of the Olympus CellSens Dimension 2.2 software (five iterations with adaptive PSF and background removal, Olympus). Maximum projections of live images containing *Hoxa1::EGFP-F*-positive cells (channel) were corrected for photo bleaching in Fiji/ImageJ.

2.6 | Temporal-color projections and kymographic analysis

Temporal-color projections were generated using Fiji/ImageJ. Kymograph analysis of axons crossing or exiting the FP as previously described (Medioni et al., 2015) using a region of interest (ROI) selection, the re-slice function and the z-projection of the re-sliced results in Fiji/ImageJ, which allowed following pixel movements within the horizontal axis. The ROI in the FP was selected as a $103 \times 51 \mu\text{m}^2$ (Figure 7(c,d)) or $103 \times 27 \mu\text{m}^2$ (Figure 7(e,f)) rectangle.

2.7 | Immunohistochemistry

Spinal cords dissected from HH22 embryos or intact spinal cords that were cultured for 1 day *ex vivo* were fixed 1 h at room temperature with 4% paraformaldehyde in PBS, washed three times for 5 min each with PBS and cryopreserved for at least 24 h at 4°C in 25% sucrose in PBS. After mounting in O.C.T. compound (Tissue-Tek) and freezing the spinal cords, $25\text{-}\mu\text{m}$ thick cryosections were collected using a cryostat. The next day, sections were blocked and permeabilized 1 h at room temperature with 5% FCS in 0.1% Triton X-100 in PBS (blocking buffer). Primary antibodies were diluted in blocking buffer and added to sections overnight at 4°C (1:400 for goat-anti-GFP-FITC, Cat# 600-102-215, RRID: AB_218187, Rockland; 1:2500 for rabbit-anti-RFP, Cat# ABIN129578, RRID: AB_10781500, antibodies-online; 1:200 for rabbit-anti-cleaved caspase 3, Cat# 9661S, RRID: AB_2341188, Cell Signaling; 1:500 for goat-anti-NrCAM, G68, polyclonal antibody produced against the full length of chicken NrCAM purified from E14

chicken brain membranes (Fitzli et al., 2000); supernatants containing monoclonal mouse antibodies obtained from DSHB: anti-Lhx2 (clone PCRP-LHX2-1C11, RRID: AB_2618817), anti-islet-1 (clone 40.2D6, RRID: AB_528315), anti-Nkx2.2 (clone 74.5A5, RRID: AB_531794), anti-Hnf3 β (clone 4C7, RRID: AB_2278498); $3.1 \mu\text{g}/\text{ml}$ of mouse-anti-Shh (clone 5E1, RRID: AB_2188307); mouse-anti-laminin-1 (clone 3H11, RRID: AB_528342); mouse-anti-BEN/SC-1 (clone BEN, RRID: AB_2314001). The next day, sections were washed three times for 15 min each at room temperature with 0.1% Triton-X100 in PBS. Primary antibodies (except anti-GFP-FITC) were detected with a 2-h incubation in adequate secondary antibodies diluted in blocking buffer (1:1000 for donkey-anti-mouse-IgG-Cy5, Cat#115-175-146, RRID: AB_2338713 or donkey-anti-rabbit-IgG-Cy3, Cat# 711-165-152, RRID: AB_2307443, both from Jackson ImmunoResearch). Finally, nuclei were counterstained for 10 min at room temperature with $2.5 \mu\text{g}/\text{ml}$ of Hoechst diluted in 0.1 Triton X-100 in PBS (Cat# H3570, Invitrogen), washed three times for 10 min each with 0.1% Triton X-100 in PBS and two times for 5 min each with PBS before mounting the slides in Mowiol/DABCO. Images were taken with an Olympus IX83 inverted microscope equipped with a spinning disk unit (CSU-X1 10,000 rpm, Yokogawa), a $\times 20$ air objective (UPLSAPO $\times 20/0.8$, Olympus) or a $\times 40$ silicon oil objective (UPLSAPO S $\times 40/1.25$, Olympus), and an Orca-Flash 4.0 camera (Hamamatsu) with the Olympus CellSens Dimension 2.2 software, or with an Olympus BX61 upright microscope and a $\times 10$ air objective (UPLFL PH $\times 10/0.30$, Olympus) or $\times 40$ water objective (UAPO W/340 $\times 40/1.15$, Olympus) and an Orca-R² camera (Hamamatsu) with the Olympus CellSens Dimension 2.2 software.

2.8 | Whole-mount immunostaining

Intact spinal cords dissected from HH24-25 embryos were fixed for 1 h at room temperature in 4% paraformaldehyde in PBS and washed three times 10 min each with PBS. Spinal cords were permeabilized and incubated for 1 h at room temperature with 5% FCS in 0.1% Triton X-100 in PBS (blocking buffer). Primary antibodies were diluted in blocking buffer and added to spinal cords for incubation overnight at 4°C (1:800 of goat-anti-GFP-FITC, Rockland; 1:5000 of rabbit-anti-RFP, antibodies-online; 1:200 of mouse-anti-laminin supernatant, clone 3H1, RRID: AB_528342, DSHB). The next day, sections were washed three times 30 min each at room temperature with 0.1% Triton-X100 in PBS. The primary antibody against RFP was detected with a 2-h incubation with donkey-anti-rabbit-IgG-Cy3 antibody (1:1000, Cat# 711-165-152, RRID: AB_2307443, Jackson ImmunoResearch) and the one against laminin with donkey-anti-mouse-IgG-Cy5 (1:1000, Cat#115-175-146, RRID: AB_2338713, Jackson ImmunoResearch) diluted in blocking buffer. Finally, nuclei were counterstained for 30 min at room temperature with $2.5 \mu\text{g}/\text{ml}$ of Hoechst diluted in 0.1% Triton X-100 in PBS (Invitrogen). Samples were washed three times 30 min each with 0.1% Triton X-100 in PBS and two times 15 min each in PBS. Stained spinal cords were mounted in $100 \mu\text{l}$ of 0.5% low-melting agarose in PBS with the ventral midline pointing down on a 35-mm Ibidi μ -dish with

glass bottom (Ibidi, #81158), similarly as described above. This allowed accessing the commissure of fixed *in vivo* samples and visualization of dl1 axons and their growth cone with an Olympus IX83 inverted microscope equipped with a spinning disk unit (CSU-X1 10,000 rpm, Yokogawa). Pictures were taken with a $\times 4$ air objective (UPLFLN PH $\times 4/0.13$, Olympus), a $\times 20$ air objective (UPLSAPO $\times 20/0.75$, Olympus)

or a $\times 40$ silicon oil objective (UPLSAPO S $\times 40/1.25$, Olympus) and an Orca-Flash 4.0 camera (Hamamatsu) with the Olympus CellSens Dimension 2.2 software. Note that the same mounting and microscopy procedure was applied to HH23-25 intact spinal cords that were not stained and were used for the quantification of average growth cone areas *in vivo* (shown in Figure 9(c)).

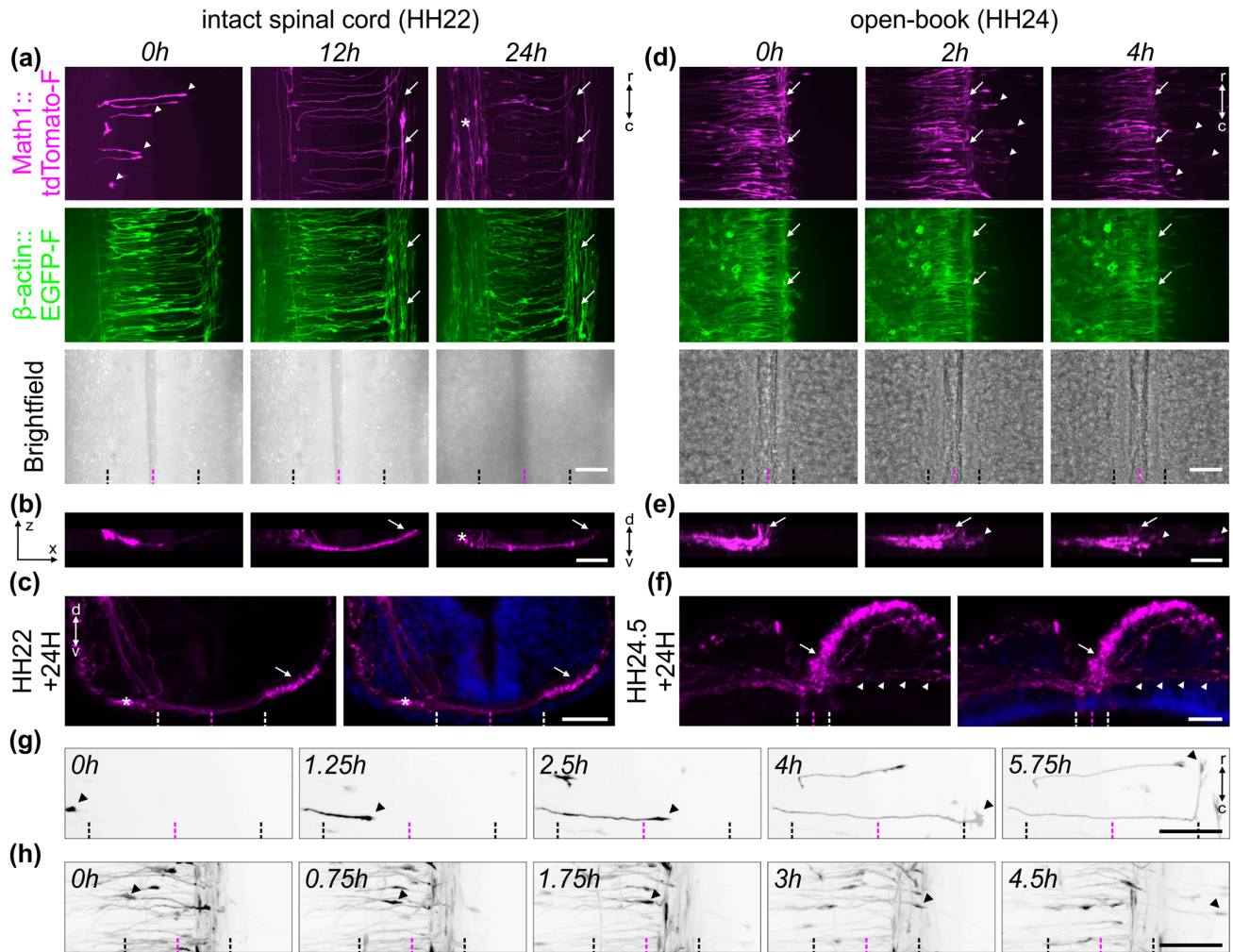


FIGURE 3 Live imaging of cultured intact spinal cords allowed for the visualization of dl1 axons during floor plate crossing and navigation into the longitudinal axis. (a) 24-h time-lapse recording showed that Math1-positive dl1 commissural axons could cross the floor plate (FP) (white arrowheads), turn anteriorly, as expected, and form the contralateral ventral funiculus (white arrows) in cultured intact HH22 spinal cords. The asterisk indicates a population of Math1-positive ipsilateral axons. (b) Transversal view of a region of interest from the time-lapse recording shown in (a), highlighting the trajectory of dl1 axons and the formation of the commissure. The white arrow indicates the position of the contralateral ventral funiculus. The white asterisk labels ipsilateral axons. (c) The normal development of the commissure could be verified by immunochemistry on transverse sections of spinal cords cultured for 24 h. Nuclei were counterstained with Hoechst (shown in blue). (d) 4-h time-lapse recording showing Math1-positive dl1 commissural axons in a cultured open-book preparation of a HH24 spinal cord. Note that within less than 2 h in culture the majority of dl1 commissural axons were overshooting the contralateral FP boundary and growing straight into the contralateral side after having crossed the FP (white arrowheads). White arrows indicate the contralateral ventral funiculus. (e) Transversal view of a region of interest from the time-lapse sequence shown in (d) highlighting the aberrant trajectory of dl1 commissural axons (white arrowheads) growing straight past the contralateral ventral funiculus (white arrow). (f) The aberrant development of the commissure could be verified by immunochemistry on transverse sections of open-books cultured for 24 h. This clearly showed dl1 axons growing straight after having crossed the FP (white arrowheads). Nuclei were counterstained with Hoechst (shown in blue). (g) Single dl1 growth cones (black arrowheads) could be tracked crossing the FP, exiting it and turning rostrally in an intact spinal cord preparation. Math1-positive axons are now shown in black. (h) Single dl1 growth cones could also be tracked crossing the FP, exiting it, but instead of turning rostrally, most of them overshoot in the contralateral part (black arrowheads). Black and white dashed lines indicate FP boundaries, magenta dashed lines the midline, respectively. d, dorsal; v, ventral; r, rostral; c, caudal. Scale bars: 50 μ m

2.9 | Shh intensity measurement in the FP

Transverse cryosections from the lumbar and the thoracic regions (see Figure 5(g)) were immunostained for Shh and counterstained with Hoechst to reveal the FP morphology (see Section 2.7). The mean intensity was measured in the FP using a circle ROI with a diameter of 100 μm . For each embryo, this intensity was

measured from two to three consecutive sections per level (lumbar and thoracic), averaged and normalized to the average intensity of the lumbar level. This was performed for four intact spinal cords and open-book preparations that were fixed after 24 h in culture. For all embryos and levels, the acquisition settings were exactly the same. Images were taken with an Olympus BX61 upright microscope and a $\times 20$ water objective (UAPO W/340 $\times 20/0.70$,

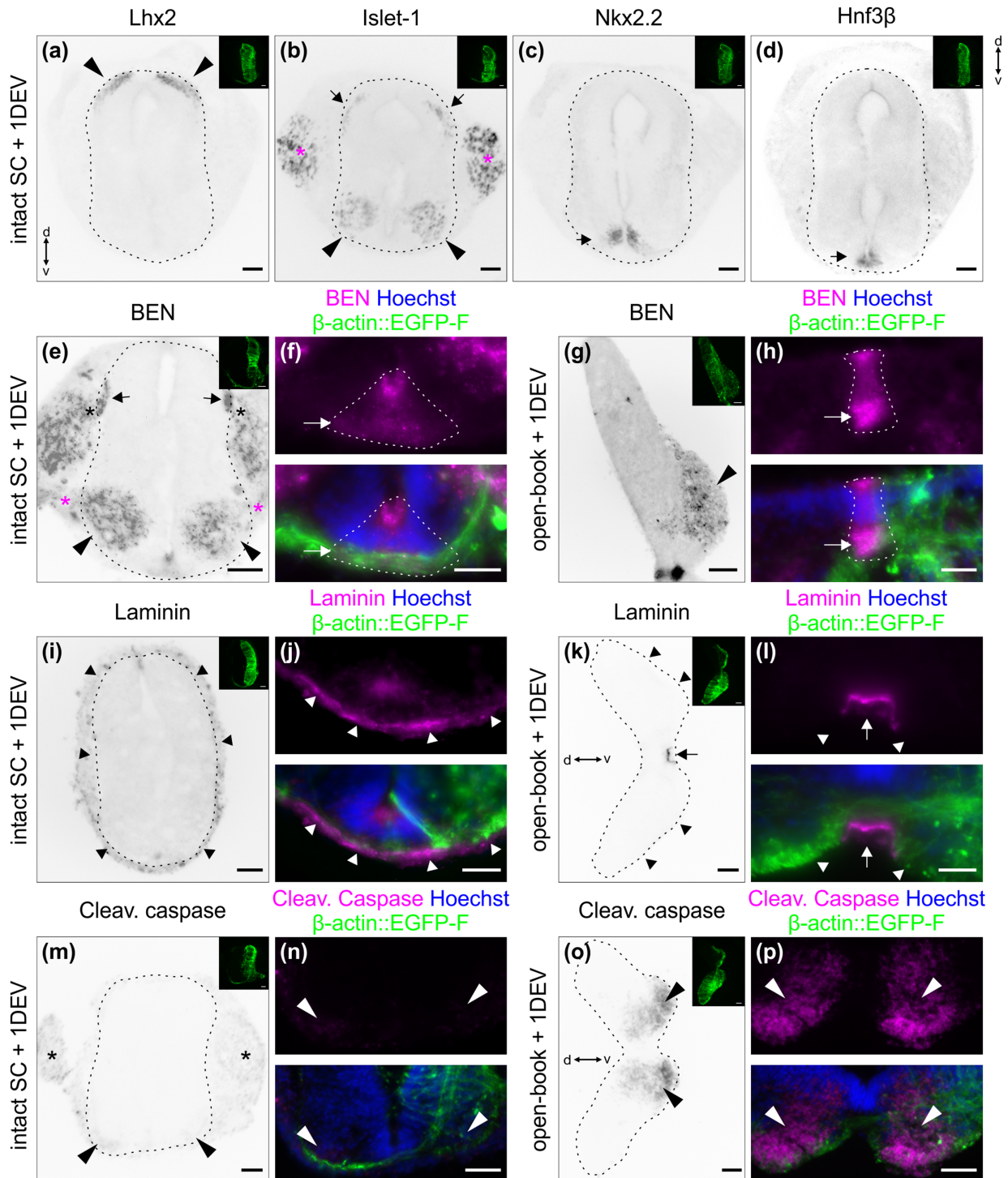


FIGURE 4 Legend on next page.

Olympus) and an Orca-R² camera (Hamamatsu) with the Olympus CellSens Dimension 2.2 software.

2.10 | Statistics and figures assembly

Statistical analyses were carried out with GraphPad Prism 7.02 software. All data were assessed for normality (normal distribution) using the D'Agostino and Pearson omnibus K2 normality test and visual assessment of the normal quantile–quantile plot before choosing an appropriate (parametric or nonparametric) statistical test. *p*-Values of the simple linear regression shown in Figure 7(i,j) demonstrate whether the slope is significantly different to zero and the dashed lines represent the 95% confidence intervals. Figures were assembled using Corel Draw 2017.

3 | RESULTS

3.1 | Electroporation is an efficient tool to selectively label dl1 neurons

We used unilateral *in ovo* electroporation of the chicken spinal cord in Hamburger and Hamilton (HH) stage 17–18 embryos to specifically express farnesylated td-Tomato (td-Tomato-F) in Math1-positive dl1 neurons, as well as farnesylated EGFP (EGFP-F) expression in their environment (Figure 2(a,b)). One day after electroporation, at HH22, embryos showed expression of td-Tomato-F restricted to dl1 neurons and EGFP-F expression in the entire half of the spinal cord, as expected (Figure 2(c)) (Wilson & Stoeckli, 2011). At this stage, most of

the Math1-positive dl1 axons approached the FP, but did not yet cross the midline, whereas other more ventral populations of commissural neurons expressing EGFP-F already projected many axons to the contralateral side of the spinal cord (white arrowheads and arrow, respectively, Figure 2(c)). For this reason, we chose HH22 as the optimal stage to start tracing dl1 axons at the midline using live imaging.

3.2 | Live imaging of dl1 axons at the midline of intact spinal cord

We extracted the intact spinal cord 1 day after electroporation (Figure 1), cultured it with the ventral midline down and imaged it with an inverted spinning disk microscope and a $\times 20$ objective (Figure 2(d–f)). Math1-positive dl1 axons crossing the FP could be visualized for at least 24 h (white arrowheads, Figure 3(a); Movies 1, 2). Within this time window, many dl1 axons crossed the midline, exited the FP, turned rostrally and formed the contralateral ventral funiculus (white arrows, Figure 3(b)). A Math1-positive ipsilateral subpopulation of axons could also be seen in these recordings as previously reported *in vivo* (Phan et al., 2010) (white asterisk, Figure 3(a)). Cultures of intact spinal cords turned out to be a very stable system as the U-shaped morphology of the commissure was preserved over time (Figure 3(b,c), Movie 2) and all major cell populations were still in place after 1 day *ex vivo* (Figure 4(a–d)). DRGs were still attached to the spinal cord via their central afferents forming the dorsal roots (black asterisks), the dorsal funiculi were intact (black arrows) and the ventral roots formed by axons of motor neurons were still pointing outward of the spinal cord as visualized by BEN (also termed ALCAM or SC-1) staining (magenta asterisks, Figure 4(e)). The same staining also

FIGURE 4 Patterning and morphology of cultured intact spinal cords were conserved after 1 day *ex vivo*. After intact HH22 spinal cords were cultured and imaged for 1 day *ex vivo*, they were fixed and transverse cryosections were immunostained for different dorsal and ventral patterning markers, and counterstained with Hoechst. (a) The dl1 interneuron marker *Lhx2* confirmed that these neurons were still localized in the most dorsal part of the spinal cord, as expected (black arrowheads). (b) *Isl1* was used as a marker for dorsal root ganglia (DRG) neurons (magenta asterisks), dl3 interneurons (black arrows) and motoneurons (black arrowheads). All of them maintained the appropriate position: clustered DRG neurons adjacent to the spinal cord; dl3 interneurons localized ventrally of dl1 interneurons; motoneurons on both sides of the ventral spinal cord. (c) *Nkx2.2* staining was used to reveal the ventral population of V3 progenitors that are just next to the FP and form the typical inverted V-shape (black arrow). (d) Finally, FP cells forming the intermediate target for dl1 axons were visualized with *Hnf3 β* staining. They were localized at the ventral midline of the spinal cord as expected (black arrow). (e) Intact spinal cord cultured for 24 h maintained morphology and localization of cell types as illustrated by staining for BEN: motor neurons (black arrowheads) and their ventral roots (magenta asterisks, the dorsal roots (black asterisks), and the dorsal funiculi (black arrows) formed by DRG afferents. (f) BEN staining also revealed that the FP maintained its triangular shape (dashed lines) and its bulky basal segment (white arrow). (g) Same staining of open-book preparations, which were cultured for the same amount of time: the motor column (black arrowhead) is stained for BEN but ventral roots and DRG afferents were removed during dissection. (h) The FP (dashed line) lost its triangular shape and its basal segment appeared to be much narrower in cultured open-books (white arrow). (i) Overview image of an intact spinal cord cultured for 24 h and stained for laminin, revealing intact meninges surrounding the spinal cord (black arrowheads). (j) Higher magnification image showing intact laminin-positive basal lamina (white arrowheads) at the ventral midline. (k) Overview image of an open-book cultured for 24 h showing the lack of meninges on the basal side of the spinal cord (black arrowheads) and a patch of meninges that remained below the FP (black arrow). (l) Higher magnification of the same section revealed that the laminin-enriched basal lamina was intact but deformed at the level of the FP (white arrow) and discontinued around it (white arrowheads). (m,n) Staining for cleaved caspase revealed a weak signal in the DRG (black asterisks) and a very weak signal in the motor column (arrowheads) of a cultured intact spinal cord. (o,p) The same staining showed a very strong signal in the ventral spinal cord of a cultured open-book (arrowheads). Hoechst was used to counterstain nuclei. The dashed black lines represent the outer border of the spinal cord. Note that small images on the upper right corner of the different panels show the β -actin::EGFP-F-electroporated side of the spinal cord. When not indicated dorsal is up. DEV, day *ex vivo*; d, dorsal; v, ventral, Cleav., Cleaved. Scale bars: 50 μ m (a–e,g,i,k,m,o) and 25 μ m (f,h,j,l,n,p)

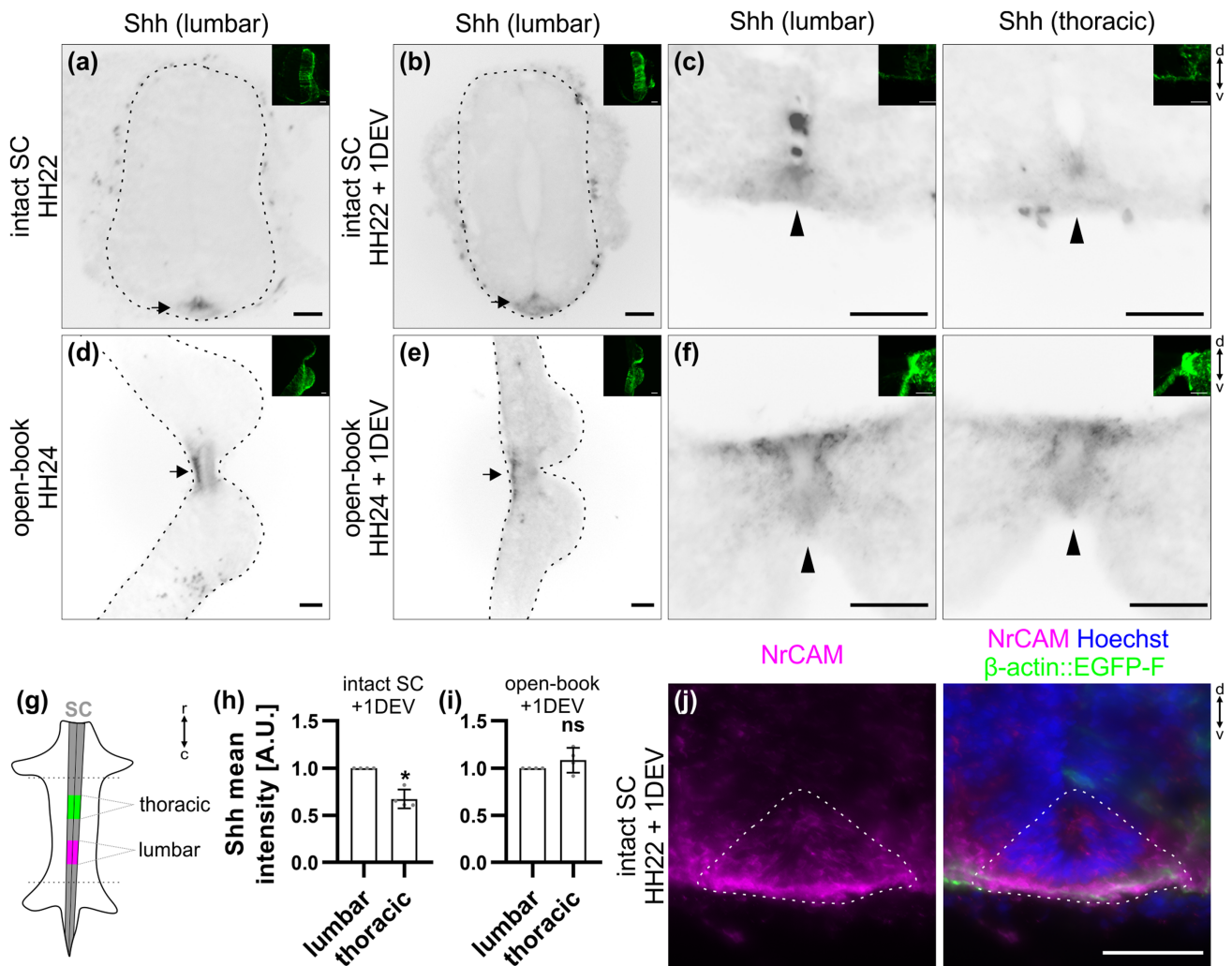


FIGURE 5 A Shh gradient is still present in cultured intact spinal cords (SCs) but not open-books after 1 day ex vivo. Intact HH22 SCs or open-books were cultured for 1 day ex vivo before fixation. Transverse cryosections were immunostained with antibodies against Shh (5E1 clone) and counterstained with Hoechst. (a,b) Shh was still expressed in the floor plate (FP) of intact SCs after 1 day ex vivo in a similar manner as right after dissection (black arrows). (c) Moreover, in agreement with previous descriptions in vivo, Shh was expressed in a decreasing caudal-to-rostral gradient with higher expression at the lumbar compared to the thoracic level (black arrowheads). (d,e) Shh was still expressed in the FP of cultured open-books (black arrows). (f) However, the gradient was lost with no more obvious difference in expression between lumbar and thoracic levels (black arrows). (g) Cartoon depicting the different levels taken for the quantification in (h) and (i). (h,i) Quantification of the mean intensity of Shh staining in the lumbar versus thoracic FP of cultured intact SCs and open-books. Note that values were normalized to the lumbar level (value = 1). (h) There was a significant decrease in the intensity of Shh in the FP of intact SC at thoracic levels (0.7 ± 0.1) compared to lumbar levels ($N = 4$ embryos). (i) However, in cultured open-books this difference disappeared (average value in thoracic level = 1.1 ± 0.1 , mean \pm SD, $N = 4$ embryos, two-tailed Mann-Whitney U test). Error bars represent SD. $p < .05$ (*) and $p \geq .05$ (ns). (j) Nrcam (shown in magenta) was still expressed in the FP (dashed line) of a cultured intact SC. Note that small images on the upper right corner of the different panels show the β -actin::EGFP-F-electroporated side of the SC. The dashed black lines represent the outer border of the SC. d, dorsal; v, ventral; r, rostral; c, caudal. Scale bars: 50 μ m

revealed that the overall triangular shape of the FP was preserved with enlarged basal structures in the commissure area (white arrow, Figure 4(f)). Furthermore, the secreted guidance cue Sonic hedgehog (Shh) was still restricted to the FP and showed the caudal (lumbar, high) to rostral (thoracic, low) gradient, like in vivo (Figure 5(a-c,g,h)) (Bourikas et al., 2005). Additionally, Nrcam, a cell adhesion molecule that guides dl1 axons into the FP, was still expressed there (Figure 5(j)) (Stoeckli & Landmesser, 1995). Most importantly, dl1 axons'

navigation was identical to the in vivo situation during this time window (Figure 6). We also compared our ex vivo method with a recently published protocol using open-book preparations of HH24-26 chicken spinal cords for the analysis of receptor dynamics to push axons out of the midline area (Pignata et al., 2019) (Figure 2(g-i)). In contrast to this protocol, our ex vivo method did not result in overshooting axons, an artifact that we have already seen after short times in cultures of open-book preparations, with Math1-positive dl1 commissural axons

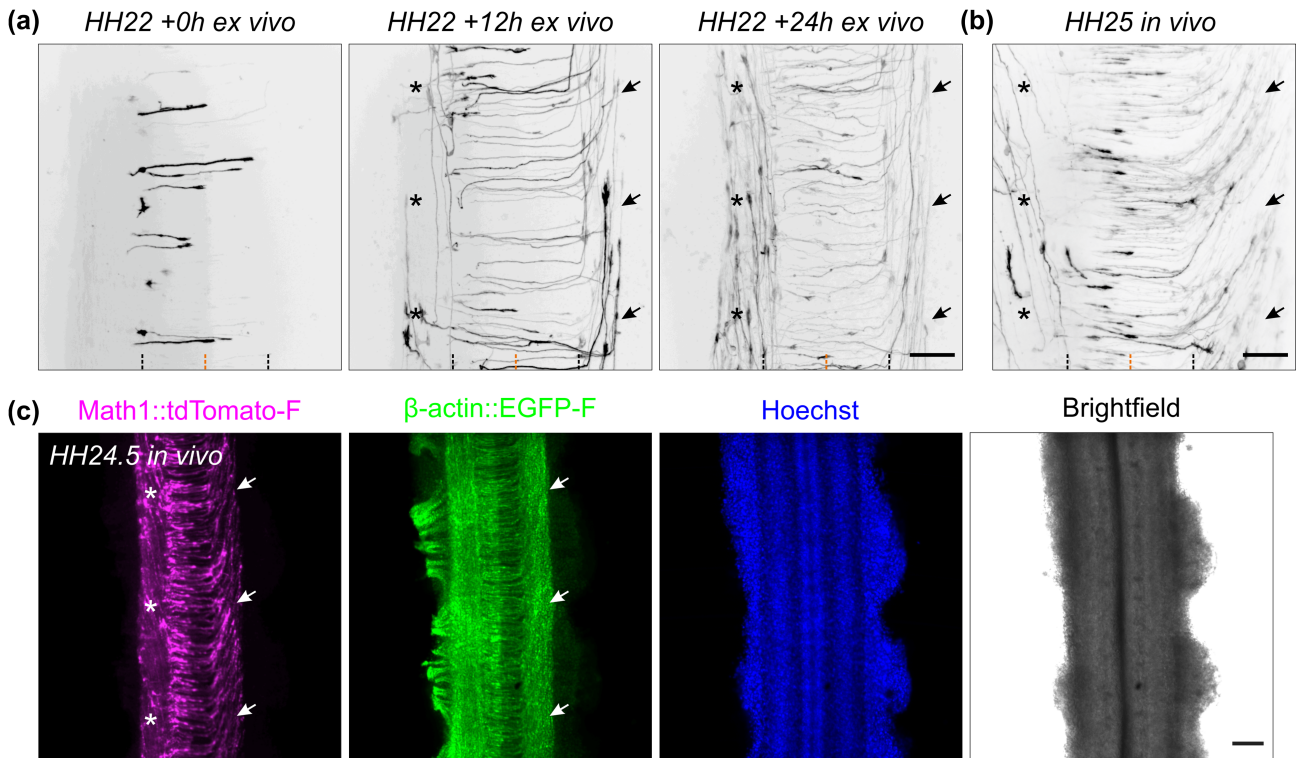


FIGURE 6 Development of Math1-positive axonal tracts ex vivo and in vivo. (a) Sequence of three images showing dl1 axons crossing the floor plate (FP) after 0, 12, and 24 h of culture. After turning rostrally, postcrossing axons started to form the contralateral ventral funiculus (black arrows). After around 12 h in culture, a Math1-positive ipsilateral population could be clearly seen in the ipsilateral ventral funiculus (black asterisks). (b) Intact spinal cords dissected at HH25 (approximately 1 day after HH22), fixed and mounted similarly to the ex vivo culture were imaged the same way. This revealed identical dl1 axonal tracts compared to those seen after 24 h of culture of intact spinal cords dissected at HH22, with postcrossing axons forming the contralateral ventral funiculus (black arrows) and ipsilateral axons turning in the ipsilateral ventral funiculus (black asterisks). Black and orange dashed lines represent FP boundaries and midline, respectively. (c) Low magnification overview of an intact HH24.5 spinal cord, fixed, stained for RFP (Math1-positive neurons) and GFP (β -actin transfected cells) and counterstained with Hoechst showing the contralateral ventral funiculus containing postcrossing dl1 axons (white arrows) and the ipsilateral ventral funiculus containing a population of ipsilateral axons (white asterisks). Scale bars: 50 μ m (a,b) and 100 μ m (c)

that crossed the midline but then failed to turn into the longitudinal axis and continued to grow straight into the contralateral side instead (white arrowheads, Figure 3(d,e); Movie 3). Because many of our studies focus on the turning behavior of postcrossing axons at the FP exit site, the high incidence of aberrant axon growth into the contralateral half of the spinal cord is not acceptable. We found that $91 \pm 6\%$ of dl1 axons overshot, whereas $8 \pm 6\%$ turned rostrally, and $1 \pm 1\%$ turned caudally at the contralateral side (mean \pm SD, $N(\text{embryos}) = 4$, $n(\text{axons}) = 392$). In our system, none of them overshot, and $98 \pm 2\%$ turned rostrally and $2 \pm 2\%$ caudally at the contralateral side (mean \pm SD, $N(\text{embryos}) = 7$, $n(\text{axons}) = 305$). Although open-book cultures offer the possibility to follow midline crossing of single dl1 axons (Figure 3(h)), we could observe a number of important differences in tissue integrity compared to intact spinal cord cultures. The observed axon guidance artifacts are most likely explained by the deformation of the FP and commissure in this preparation (Figures 3(e,f) and 4(h)) and the fact that diffusible guidance cues are not well retained in the tissue, as exemplified by Shh that lost its caudal (lumbar) to rostral (thoracic) gradient after 24 h in culture (Figure 5(d-f,g,i)).

In line with this, staining for laminin revealed that the meninges surrounding the spinal cord were intact in our culture system (black arrowheads, Figure 4(i)) but mostly absent from open-book preparations (black arrowheads, Figure 4(k)), where only an isolated patch remained at the FP (black arrow, Figure 4(k)). Meninges secrete extracellular matrix proteins that are deposited in and organize the basal lamina surrounding the spinal cord (Siegenthaler & Pleasure, 2011). The integrity of the basal lamina and the secreted guidance molecules that are localized in it were shown to play a crucial role in guidance of commissural axons at the ventral midline of the spinal cord (Burstyn-Cohen et al., 1999; Wright et al., 2012; Zisman et al., 2007). The laminin staining also revealed that the basal lamina was intact at the commissure of cultured intact spinal cord (white arrowheads, Figure 4(j)), whereas it was deformed (white arrow) and discontinued in cultured open-books (white arrowheads, Figure 4(l)). We also assessed possible apoptosis in cultured intact spinal cords by staining for cleaved caspase. We found very little apoptosis in the ventral spinal cord (arrowheads, Figure 4(m,n)) and DRGs in our system (black asterisks, Figure 4(m)). In contrast, cultured open-books showed massive

apoptosis in the ventral spinal cord (arrowheads, Figure 4(o,p)) in the region of the motor columns that might be caused in part by the complete loss of ventral roots in this system (black arrowhead, Figure 4(g)). A combination or all of these marked differences observed in cultured open-books are likely to be responsible for the strong artificial behavior of dl1 axons at the contralateral FP border. In contrast, our ex vivo method of culturing intact spinal cords offers a highly stable intact system in which dl1 commissural axons are behaving as expected based on what is known from in vivo studies with the advantage that individual axons can be followed during midline crossing and subsequent turning along the contralateral FP border.

3.3 | Characterization of the timing of midline crossing by dl1 commissural axons

The time it takes commissural axons to cross the FP has been estimated but could not be measured exactly (Stoeckli, 2018; Zou, 2012). However, timing is an issue, because axons have to change their responsiveness to FP-derived guidance cues, like the Slits, Shh, or Wnt proteins, by expressing appropriate receptors in a precisely regulated manner (Bourikas et al., 2005; Domanitskaya et al., 2010; Long et al., 2004; Lyuksyutova et al., 2003; Philipp et al., 2012; Wilson & Stoeckli, 2013). With our method, we could track single dl1

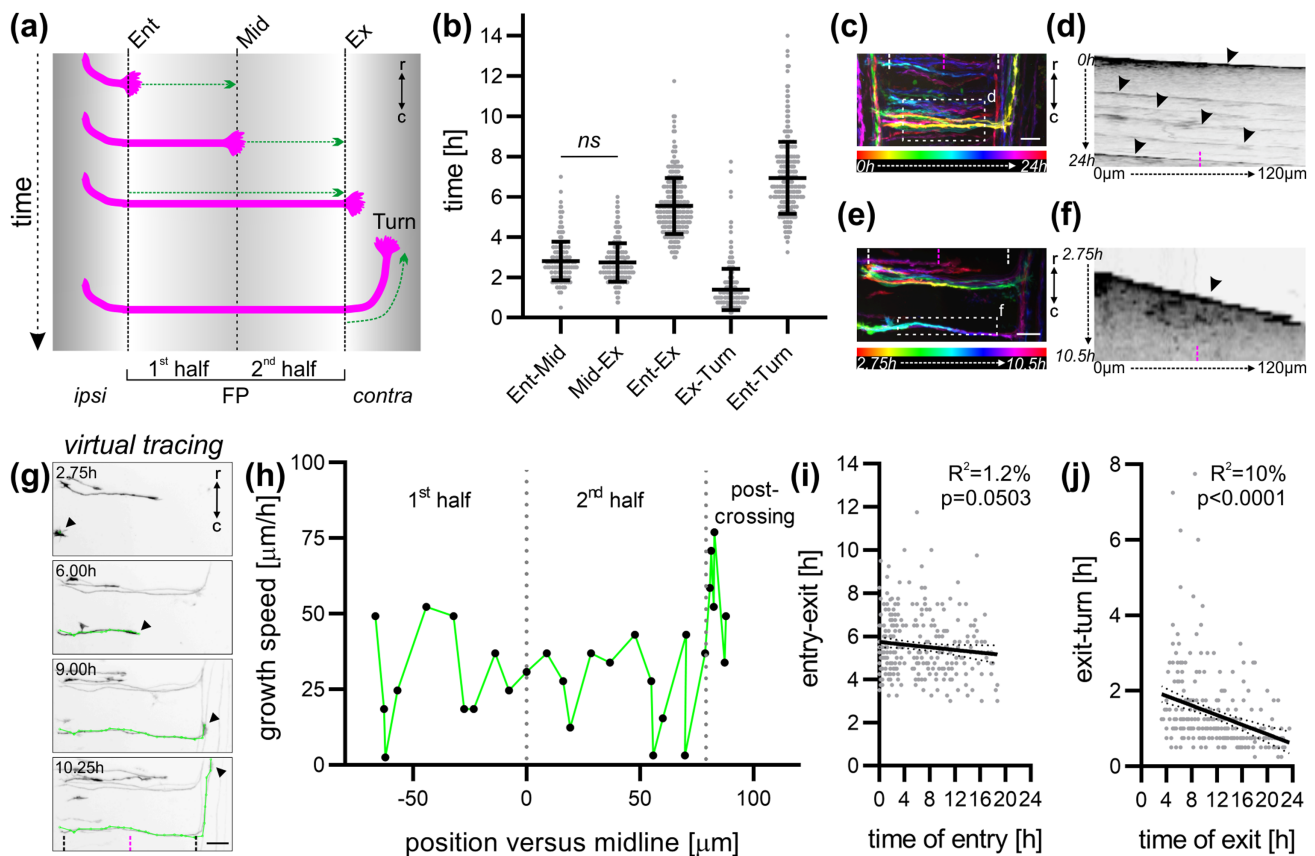


FIGURE 7 Characterization of the timing of midline crossing by dl1 commissural axons. (a) Schematic depicting how the timing of midline crossing for individual dl1 axons was measured for each segment of interest. (b) Graph showing the average time a growth cone spent in each segment shown in (a) ($N_{\text{embryos}} = 7$; $n_{\text{axons}} = 298$). There was no significant difference in the time taken by dl1 axons to cross the first versus the second half of the floor plate (FP) ($p \geq .05$, paired two-tailed Wilcoxon test). (c) Temporal-color code projection of a 24-h time-lapse recording. (d) Kymograph of the 24-h time-lapse recording in the region of interest within the FP shown in (c). Several axons crossing the FP at different times can be visualized (black arrowheads). (e) Temporal-color code projection of 7.75-h time-lapse recording segment. (f) Kymograph of the 7.75-h time-lapse recording segment in the region of interest within the FP shown in (e). Within this time segment, only one axon crossed the FP and could be visualized in the kymograph (black arrowhead). White and magenta dashed lines represent the FP boundaries and the midline, respectively. (g) A virtual tracing tool (shown in green) was used to extract the velocity of the growth cones (black arrowheads) at each time point during midline crossing at the single axon level. The same axon is shown in (e) and (g). Black dashed lines and the magenta dashed lines represent the FP boundaries and midline, respectively. (h) The growth speed of the axon shown in (g) could be extracted and plotted against the position of the growth cone in the FP. Dotted gray lines represent the time at which the axon crossed the midline or exited the FP. (i,j) The time of crossing the FP (entry-exit) or of turning (exit-turn) for each axons measured in (b) was plotted against the time of FP entry and exit of the growth cone, respectively. (i) The time axons took to cross the FP appeared to decrease over time although this was not significant. (j) The time axons took to turn after exiting the FP decreased significantly over time. ipsi, ipsilateral; contra, contralateral; Ent, entry; Mid, midline; Ex, exit; r, rostral; c, caudal. Scale bars: 25 μm

Figure	Name	Mean	SD	
Figure 7(b)	Ent-Mid	2.81	0.96	$n(\text{axons}) = 298, N(\text{embryos}) = 7$
	Mid-Ex	2.74	0.95	$n(\text{axons}) = 298, N(\text{embryos}) = 7$
	Ent-Ex	5.55	1.39	$n(\text{axons}) = 298, N(\text{embryos}) = 7$
	Ex-Turn	1.39	1.03	$n(\text{axons}) = 298, N(\text{embryos}) = 7$
	Ent-Turn	6.94	1.79	$n(\text{axons}) = 298, N(\text{embryos}) = 7$
Figure 9(b)	First half	46.1	12.2	$n(\text{growth cones}) = 127, N(\text{embryos}) = 7$
	Second half	44.2	11	$n(\text{growth cones}) = 127, N(\text{embryos}) = 7$
	Exit	105.5	25	$n(\text{growth cones}) = 127, N(\text{embryos}) = 7$
	After turn	67.8	17.6	$n(\text{growth cones}) = 127, N(\text{embryos}) = 7$
Figure 9(c)	First half	41	12.6	$n(\text{growth cones}) = 285, N(\text{embryos}) = 8$
	Second half	41.8	11.5	$n(\text{growth cones}) = 153, N(\text{embryos}) = 8$
	Exit	116.9	25.7	$n(\text{growth cones}) = 68, N(\text{embryos}) = 8$
	After turn	76.5	18.9	$n(\text{growth cones}) = 102, N(\text{embryos}) = 8$

TABLE 1 Detailed values shown in Figures 7 and 9

commissural axons in the FP at any time point and in different ROIs (black arrowheads, Figure 3(g)). We were therefore able to ask, how long dl1 axons needed for FP crossing and their subsequent rostral turn (Figure 7(a)). On average, dl1 commissural axons took 5.6 ± 1.4 h to cross the entire FP and 1.4 ± 1.0 h to turn and initiate the rostral growth at the FP exit site. Thus, in total, they needed 6.9 ± 1.8 h from entering the FP to the initiation of their rostral growth (mean \pm SD, Figure 7(b) and Table 1). There was no significant difference between the average time of crossing the first versus the second half of the FP (Figure 7(b), Table 1). This was supported by kymographic analysis of a ROI within the FP from 24-h time-lapse recordings showing similar growth patterns between the first and second half of the FP at the single axon level (Figure 7(c), black arrowheads in Figure 7(d), Movie 4). Although the kymographic analysis was useful to screen for overall growth pattern of single dl1 axons within the FP (Figure 7(e,f)), it was not sensitive enough to detect more subtle changes in growth speed. Hence, we used a virtual tracing tool to follow the movement of the leading edge of each growth cone at each time point (Figure 7(g)). With this tool, we could extract the local growth speed for each axon at a specific time point (defined as the average speed during the previous 15 min). It turned out that the large majority of them had a fluctuating growth pattern with random acceleration–deceleration pulses that could be observed in early as well as late crossing axons (Figure 7(h), Movie 5, Figure 8). Another interesting observation was made when we compared the times of crossing the FP and the initiation of rostral growth after turning. There was no significant difference in the time of FP crossing of later versus earlier crossing axons ($p = .0503$; Figure 7(i)). However, the time dl1 axons took to turn rostrally at the exit site was significantly reduced over time (Figure 7(j)). The latter observation suggests that commissural axons that already turned anteriorly at the contralateral FP exit site might help the following ones to turn more rapidly. Our method offers new opportunities for further investigations of possible collaborations between axons at choice points.

3.4 | Characterization of the dl1 growth cone morphology at choice points

Another aspect that we considered was growth cone morphology. The growth cone plays a central role in axon guidance, as it explores the environment for guidance cues and translates this information into the directionality of growth (De Ramon Francàs et al., 2017; Stoeckli, 2018). In agreement with published live imaging studies from the visual system, where growth cone morphology was recorded at the chiasm (Godement et al., 1994; Sretavan & Reichardt, 1993), we found changes in growth cone morphology during midline crossing in the spinal cord. We observed that dl1 growth cones in the FP appeared to have a thin and elongated shape in the direction of growth. At the FP exit site, they transiently enlarged (arrowheads, Figure 9(d), Movie 2). We measured the average growth cone area in each segment of interest and confirmed that growth cones at the exit site of the FP were indeed significantly larger than the ones within the FP or after the turn (Figure 9(a,b), Table 1). There was no significant change in the average growth cone area between the first and second half of the FP (Figure 9(b), Table 1). The changes of growth cone shape were in line with previous reports on chicken and rat commissural axons in vivo (Bovolenta & Dodd, 1990; Yaginuma et al., 1991) and our data on Math1-positive axons in vivo (Figure 9(c), Table 1, Figure 6(b)). The possibility to follow individual axons over time allowed us to make novel observations of their behavior at the FP exit site. One hundred percent of the observed growth cones extended long filopodia in both rostral and caudal direction just before turning ($N(\text{embryos}) = 7, n(\text{axons}) = 305$, Figure 9(d), Movies 6 and 7). We observed $16 \pm 8\%$ of the growth cones to transiently split just before turning rostrally, similar to dorsal root ganglia central afferents in the mouse dorsal root entry zone before bifurcating (Dumoulin et al., 2018) (mean \pm SD, $N(\text{embryos}) = 7, n(\text{axons}) = 305$, Movie 8). All these features are present in vivo, as similar growth cone morphologies were found in fixed HH24–25 spinal cords (Figure 9(e)).

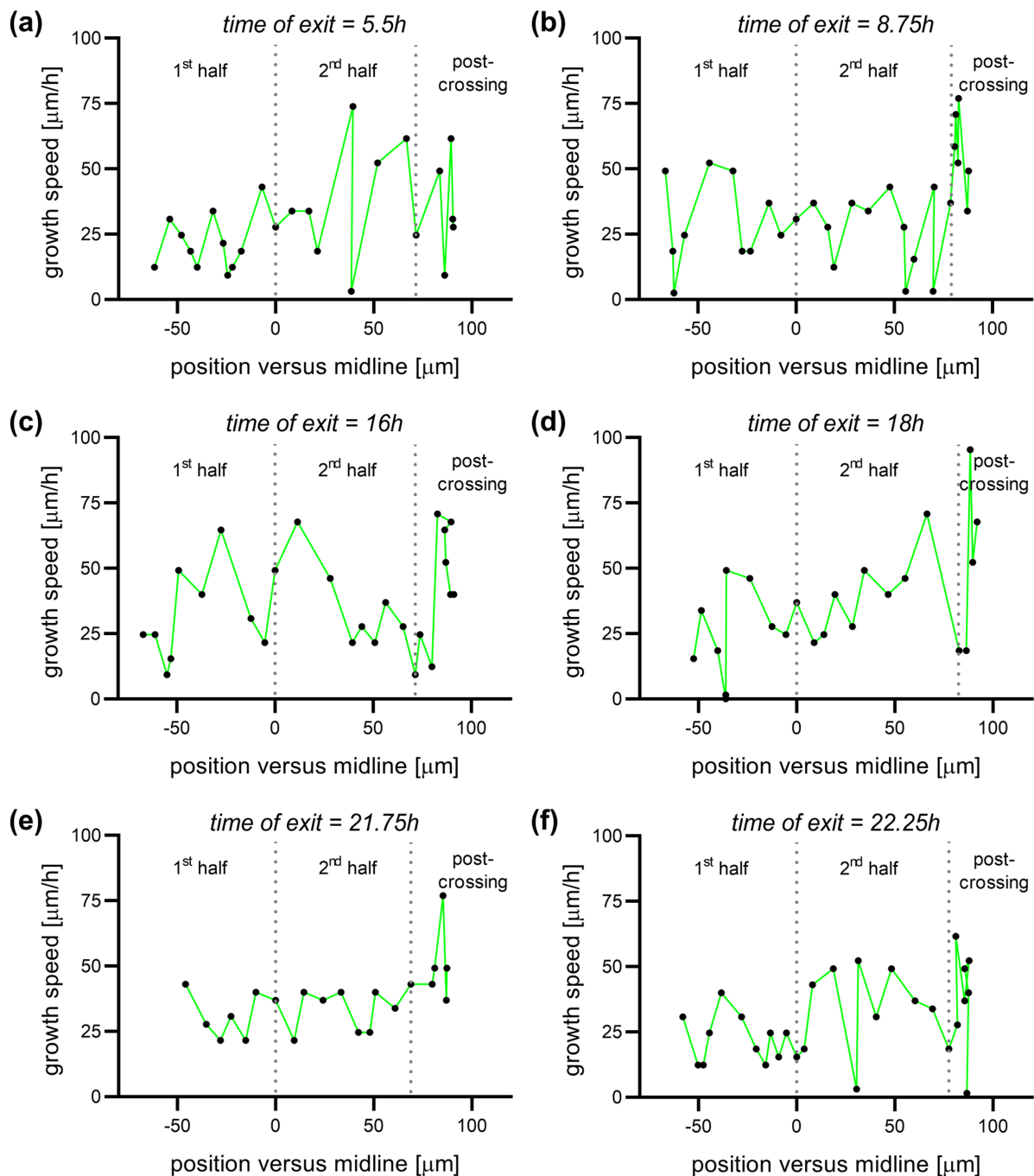


FIGURE 8 Virtual tracing of axons exiting the floor plate (FP) at different time points. Examples of local growth speed at different time points of axons exiting the FP after 5.5 h (a), 8.75 h (b), 16 h (c), 18 h (d), 21.75 h (e), or 22.25 h (f) of culture plotted against the position of the growth cone in the FP. Dotted lines represent the time at which the axon crossed the midline or exited the FP. All axons were growing with pulses of acceleration and deceleration. There was no difference between early or late crossing axons

Thus, ex vivo live imaging of cultured intact spinal cords using low magnification time-lapse microscopy offers the opportunity to detect morphological changes of growth cones at choice points and is ideal for the analysis of many aspects of midline crossing in a relative large cohort of axons. However, the limited resolution especially in 3D might preclude the detection of more subtle changes in morphology of growth cones while crossing the midline.

3.5 | Higher magnification analysis of commissural axons crossing the midline revealed dorso-ventral activities of their growth cone

For this reason, we repeated time-lapse recordings of cultured intact spinal cords using a higher magnification objective and advanced 3D deconvolution technology. This allowed following Math1::tdTomato-

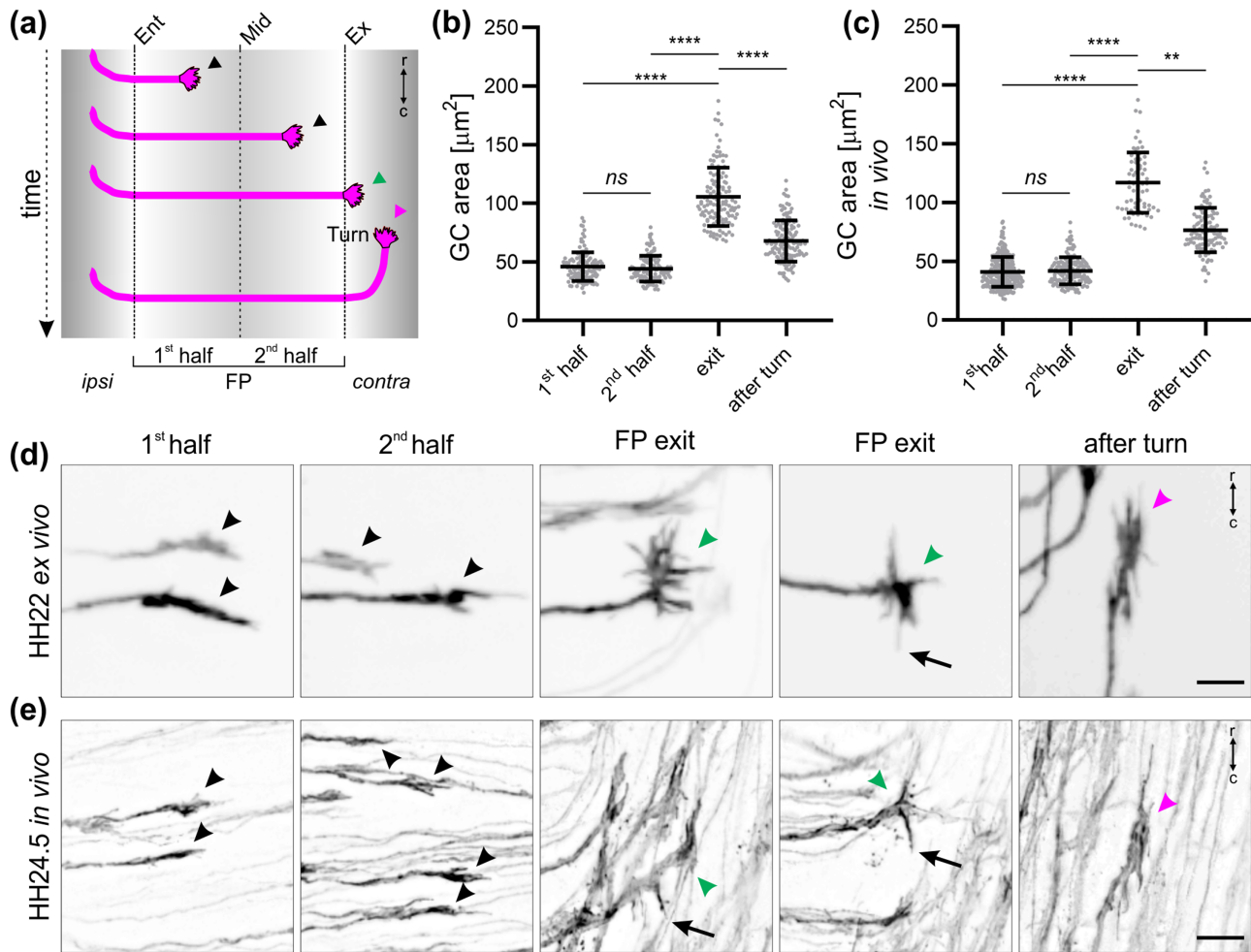


FIGURE 9 Live imaging of intact spinal cords revealed d11 growth cone morphologies at chosen time points. (a) Schematic depicting where the growth cone area of individual d11 axons was measured for (b) and (c). (b) Average growth cone areas were measured from 24-h time-lapse recordings of d11 axons crossing the midline ($N_{\text{embryos}} = 7$; $n_{\text{growth cones}} = 127$). No significant difference in the area of growth cones was found between the first and second half of the floor plate (FP). However, growth cones were significantly larger at the exit site but then again reduced in size after having turned rostrally (paired Friedman test with Dunn's multiple-comparisons test). (c) Average growth cone areas were measured in vivo from fixed HH23–25 spinal cords ($N_{\text{embryos}} = 8$; $n_{\text{growth cones}} = 285$ (first half), 153 (second half), 68 (exit), and 102 (after turn)). The relationship between the average growth cone area and the position in the FP corroborated results using the ex vivo culture system shown in (b) (unpaired Kruskal–Wallis test with Dunn's multiple-comparisons test). (d,e) Examples corroborating the similarities in growth cone morphology ex vivo and in vivo in the FP (black arrowheads), at the exit site (green arrowheads) and after rostral turn (magenta arrowheads). At the exit site, growth cones were spiky with always some filopodia pointing caudally just before rostral turn, a feature that was also observed in vivo (black arrows). ipsi, ipsilateral; contra, contralateral; r, rostral; c, caudal. Error bars represent SD. $p < .0001$ (****), $p < .01$ (**), and $p \geq .05$ (ns) for all tests. Scale bars: 10 μm

F-positive d11 axons over time while entering, crossing and exiting the FP (Movie 9). We observed that d11 growth cones crossing the FP were bulkier in the dorso-ventral axis (white arrowheads, Figure 10(a), Movie 10) and were particularly dynamic in this axis showing rapid extension of filopodial protrusions (white arrows in Figure 10(a) and Movie 10). This aspect of d11 growth cone behavior in the FP was supported by visualization of tdTomato-F-expressing growth cones and the basal lamina marker laminin as a ventral commissure reference point of HH22–24.5 whole-mount spinal cords or cryosections (arrowheads, Figure 10(b–d), Movies 11 and 12). In line with their dorso-ventral activity, we could observe that 100% of the observed d11

growth cones in the commissure sent at least once a dynamic long protrusion (up to $\sim 13 \mu\text{m}$) into the FP while crossing it (black arrow, Figure 10(e), black arrowheads, Movie 13, $N(\text{embryos}) = 4$, $n(\text{axons}) = 116$). Protrusions entering the FP could also be detected for d11 growth cones in vivo as revealed by immunostaining of HH22–24.5 whole-mount spinal cords or cryosections (white arrows, Figure 10(f,g)). Next, we also had a closer look at the FP exit site, where growth cones need to read longitudinal gradients to initiate the rostral turn after exiting the FP (Pignata et al., 2019; Stoeckli, 2018). Intriguingly, we detected that just before exiting the FP, d11 growth cones very often sent a long protrusion into the FP (arrow, Figure 10

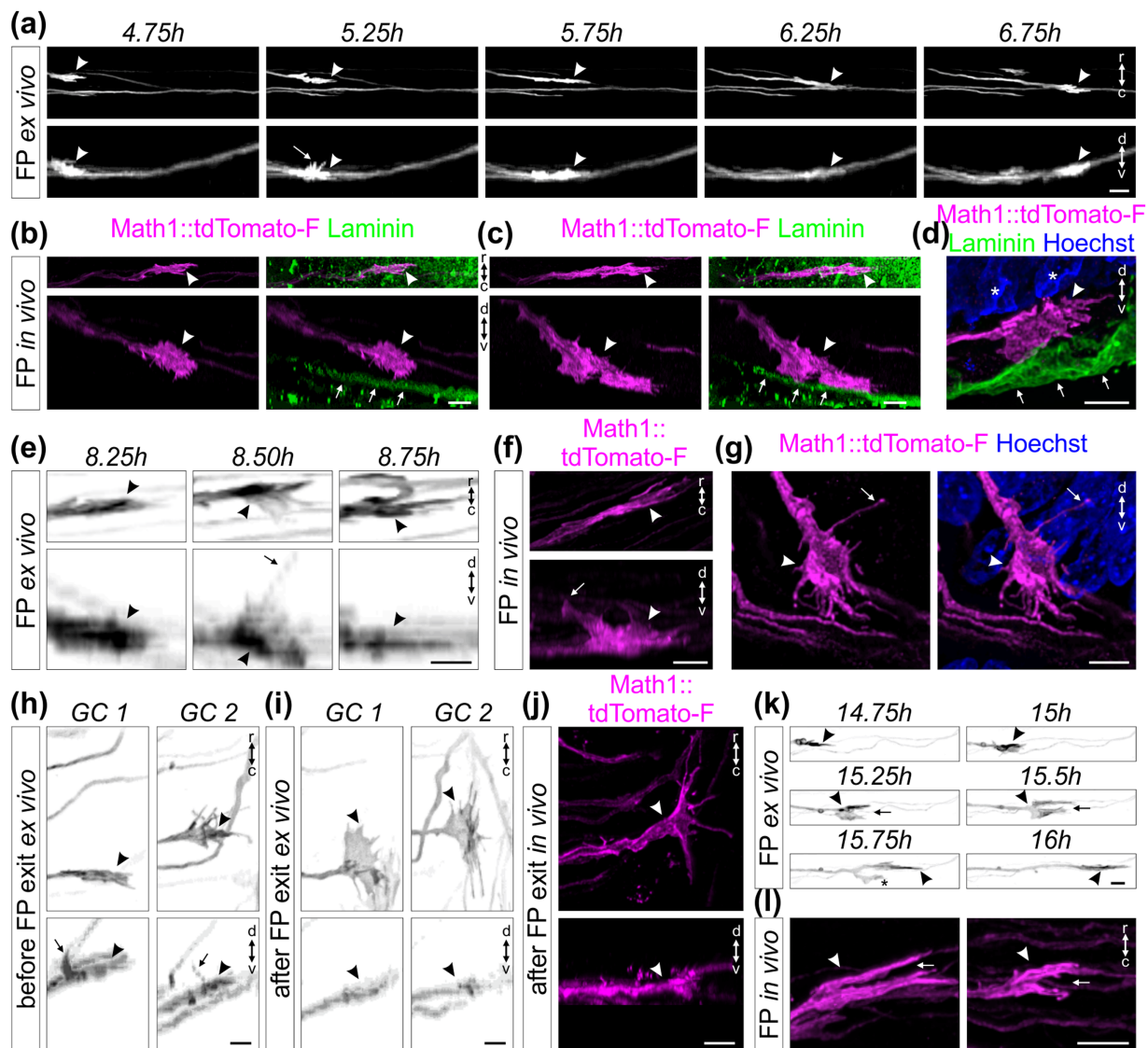


FIGURE 10 High magnification live imaging of dl1 commissural axons unraveled their orientation and activities at choice-points. (a) A Math1::tdTomato-F-positive growth cone (white arrowheads) crossing the floor plate (FP) shown in the rostro-caudal and dorso-ventral axis. White arrow shows the dorso-ventral orientation of the growth cone with some filopodia extended toward the apical FP. (b,c) Whole-mount immunostaining of Math1::tdTomato-F-positive dl1 growth cones in the FP at HH24.5 showed their dorso-ventral orientation in vivo (white arrowheads). The basal lamina was stained for laminin (white arrows). (d) A Math1::tdTomato-F-positive dl1 growth cone in the FP (white arrowhead) at HH22 showed its dorso-ventral orientation in vivo (white arrowheads). The basal lamina was stained for laminin (white arrows) and nuclei with Hoechst. White asterisks show nuclei from the FP cells. (e) Three consecutive snapshots from a time-lapse sequence showing the dorso-ventral activity of a Math1::tdTomato-F-positive growth cone crossing the FP (black arrowheads) with a long protrusion growing toward the FP soma level (black arrow). (f,g) A long protrusion growing toward the apical FP cell soma area (white arrows) could be also observed in dl1 growth cones crossing the FP in vivo (white arrowheads) after whole-mount staining of a HH24 spinal cord (f) or immunostaining on a HH22 spinal cord transverse section (g). (h) Example of two growth cones extracted from a time-lapse recording (black arrowheads) showing dorsal activity with a long protrusion (black arrows) growing toward the FP soma area just before exiting the FP. (i) The same growth cones shown in (h) after exiting the FP underwent a 90° change in their orientation. They now were thin in the dorso-ventral axis and enlarged in the rostro-caudal axis (black arrowheads). (j) HH24.5 whole-mount immunostaining of Math1::tdTomato-F-positive dl1 growth cone at the FP exit site showed that the orientation of postcrossing growth cones in vivo were the same as observed by live imaging (white arrowheads). (k) Example of a Math1::tdTomato-F-positive dl1 growth cone (black arrowhead) transiently splitting (black arrow) while crossing the FP. One branch always retracted (black asterisk) while the other one continued to grow straight to the contralateral side. (l) Split growth cones (white arrow) of Math1::tdTomato-F-positive dl1 axons (white arrowheads) could be observed in vivo after whole-mount staining of HH24.5 spinal cords. GC, growth cone; r, rostral; c, caudal; d, dorsal; v, ventral. Scale bars: 10 μm (a) and 5 μm (b–l)

(h), Movies 14, 63% of 32 growth cones that could be followed at the exit site, $N(\text{embryos}) = 4$. Live imaging clearly revealed that the activity and orientation of growth cones switched by about 90° after

exiting the FP, as they flattened in the dorso-ventral axis and enlarged in the longitudinal axis ex vivo and in vivo (Figure 10(i,j), Movie 15). Another unexpected observation we made was that $80 \pm 2\%$ of dl1

growth cones transiently split while crossing the FP (mean \pm SD, N (embryos) = 4, n (axons) = 116, asterisks in Movie 13). The splitting created two more or less equal branches (black arrows, Figure 10(k), Movie 16), but only one persisted and grew straight to the contralateral side, while the other one was retracted (black asterisks, Figure 10(k), Movie 16). Also this behavior was supported by snapshots from *in vivo* behavior of dl1 growth cones (arrows, Figure 10(l)). Taken together, *ex vivo* live imaging combined with high magnification analysis of growth cone dynamics allowed us to characterize the behavior of dl1 growth cones at choice points in more detail.

3.6 | Live imaging unraveled the dynamics and morphologies of FP cells during midline crossing

The orientation of dl1 growth cones as well as their behavior during FP crossing suggested that they have to squeeze their way between the basal feet of FP cells which are attached to the basal lamina (Yaginuma et al., 1991; Yoshioka & Tanaka, 1989). Moreover, very little was known about the morphology of FP cells during axonal midline crossing and their potential active contribution in this process has never been addressed (Campbell & Peterson, 1993; Yaginuma

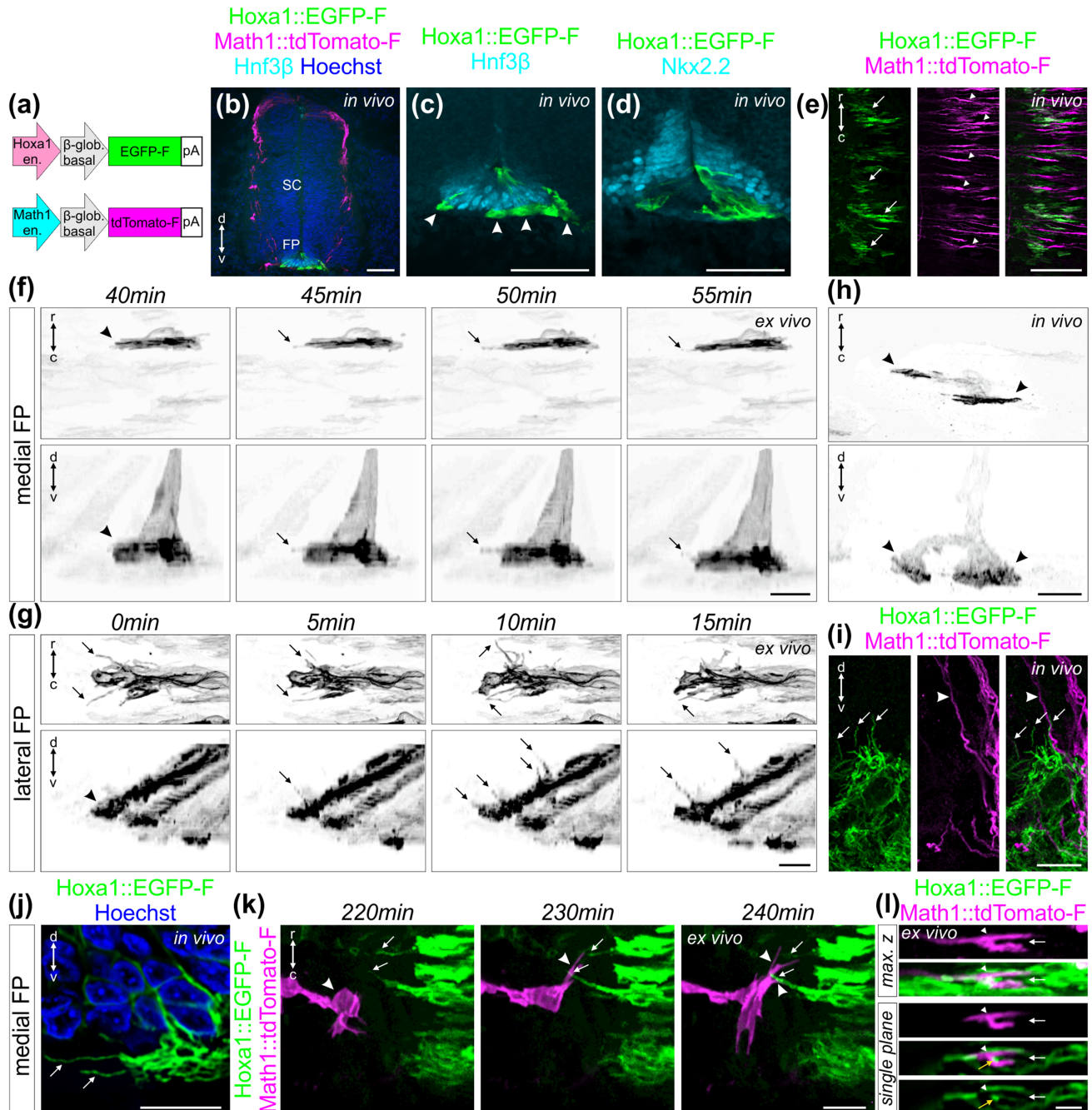


FIGURE 11 Legend on next page.

et al., 1991; Yoshioka & Tanaka, 1989). Therefore, we examined the behavior and morphology of FP cells during midline crossing in our ex vivo system. We electroporated spinal cords at HH17-18 after injection of a plasmid encoding EGFP-F under the FP-specific *Hoxa1* enhancer for expression of the membrane-bound fluorescent protein in FP cells (Li & Lufkin, 2000; Wilson & Stoeckli, 2011; Zisman et al., 2007) (Figure 11(a-d)). With this we were able to see *Hoxa1::EGFP-F*-positive bulky FP basal feet in the commissure in vivo (white arrowheads, Figure 11(c)) as well as their thin morphology and orientation (white arrows) that seemed to be tightly aligned with dl1 growth cones crossing the midline (white arrowheads, Figure 11(e)). The morphology of medial FP basal feet with little extension in the rostro-caudal axis but enlarged in the dorso-ventral axis could be observed in real time using our ex vivo culture technique (Figure 11(f), Movie 17). Interestingly, we could observe dynamic protrusions sprouting from the basal feet in direction of axonal growth in the commissure (black arrows, Figure 11(f), Movie 17). Similar observations were made for basal feet of lateral FP cells (black arrow, Figure 11(g)). They produced dynamic protrusions toward the FP entry zone at high frequency (black arrows, Figure 11(g), Movie 18). Importantly, we could observe a similar morphology of medial FP basal feet at the single-cell level in vivo (arrowheads, Figure 11(h), Movie 19). The dl1 commissural axons had the same orientation as the FP basal feet and seemed to grow in between these feet and interact with them in vivo (Movies 19 and 20). Moreover, we could observe similar protrusions coming either from lateral FP basal feet (white arrows) going toward precrossing dl1 axons arriving at the FP (white arrowheads, Figure 11(i)), or from medial FP basal feet extending parallel to axons in the commissure (white arrows, Figure 11(j) and Movie 21). The tight interaction between dl1 axons and FP basal feet during midline crossing was unexpected (Movie 21). The observation that protrusions from lateral FP basal feet (white arrowhead) were extending and contacting dl1 growth cones before they entered the FP (white arrows)

suggested a much more active role of FP cells than anticipated (Figure 11(k), Movie 22). Last but not least, we could confirm that FP basal feet structures (yellow arrow) were present in between transiently splitting dl1 growth cones (white arrowheads and arrows) in the commissure (Figure 11(l), Movie 23). Taken together, these data showed for the first time the detailed morphology of single FP cells, their dynamics and tight interactions with axons during midline crossing, and they emphasized the probable active role of FP cells in initiating contacts with growth cones before and during midline crossing.

3.7 | Trajectory and behavior of dl1 axons can be visualized in real time at choice points

Our ex vivo culture method not only offers great opportunities to characterize behavior of growth cones and FP cells in a preserved system, but it also opens new possibilities for tracking axonal behavior after specific perturbations of either the neurons or their environment. As example, the Wnt receptor *Fzd3* (*Frizzled-3*) was specifically downregulated in *Math1*-positive dl1 neurons (Alther et al., 2016; Wilson & Stoeckli, 2011) (Figure 12(a)). *Fzd3* is required for the rostral turn of postcrossing commissural axons at the contralateral FP border in vivo (Alther et al., 2016; Lyuksyutova et al., 2003). We used our ex vivo culture system to visualize *Math1::EGFP-F*-positive dl1 axons expressing a microRNA for *Fzd3* (*miFzd3*, Figure 12(b,c)). This allowed us to follow in real time how dl1 growth cones were turning caudally instead of rostrally at the contralateral FP border (black arrowheads, Figure 12(b); Movies 24 and 25). Interestingly, many axons were found to turn erroneously in caudal direction at the same position, suggesting that axons were influenced by close contact with other axons although a purely cell-autonomous effect of a loss of *Fzd3* cannot be ruled out with this experimental set up (black asterisk and black arrows in Movie 24). In addition, some axons were found stalling at

FIGURE 11 Live imaging of floor plate cells during midline crossing shed light on their orientation and dynamics. (a) Schematic depicting plasmids that were electroporated at HH17-18 to visualize floor plate (FP) cells (*Hoxa1* plasmid) together with dl1 axons (*Math1* plasmid). (b) Immunostaining of HH22 spinal cord cryosections revealed the restricted expression of *Hoxa1::EGFP-F* in FP cells co-stained for *Hnf3 β* . (c) Higher magnification of the section shown in (b) revealing *Hnf3 β* -positive FP cells expressing EGFP-F. Bulky FP basal feet could be observed in the commissure (white arrowheads). (d) Immunostaining of HH22 spinal cord cryosections showing that EGFP-F expression driven by *Hoxa1* enhancer was mostly absent in *Nkx2.2*-positive cells flanking the FP. (e) Whole-mount immunostaining of *Math1::tdTomato-F*-positive dl1 axons and *Hoxa1::EGFP-F*-positive FP cells revealed an alignment between dl1 growth cones (white arrowheads) and basal feet of FP cells (white arrows) in the commissure. (f) Example of a time-lapse recording of a single medial *Hoxa1::EGFP-F*-positive FP cell to reveal the geometry of its basal foot that was thin along the rostro-caudal axis but enlarged in the dorso-ventral axis (black arrowheads). The basal foot was highly dynamic with protrusions sprouting out in the directions of axonal growth in the commissure (black arrows). (g) Example of a time-lapse recording of lateral *Hoxa1::EGFP-F*-positive FP cells showing a very high activity of their basal feet with highly dynamic protrusions growing toward the arriving precrossing axons (black arrows). (h) Whole-mount immunostaining of a single medial *Hoxa1::EGFP-F*-positive FP cell in vivo at HH24.5 showing similar shape (black arrowheads) as observed by live imaging. Note that this FP cells contained two feet (black arrowheads). (i) Immunostaining of a HH22 spinal cord cryosection revealed that lateral *Hoxa1::EGFP-F*-positive FP cells also formed protrusions growing toward the precrossing axons in vivo (white arrows) where *Math1::tdTomato-F*-positive axons enter the FP (white arrowheads). (j) Similar protrusions were observed in HH22 medial FP basal feet in the commissure in vivo using immunostaining of cryosections (white arrows). The picture shows a single plane extracted from a Z-stack. (k) Snapshots extracted from a time-lapse sequence of a *Math1::tdTomato-F*-positive dl1 growth cone interacting (white arrowheads) with protrusions from *Hoxa1::EGFP-F*-positive FP basal feet (white arrows) before entering the FP. (l) Single snapshot from a time-lapse recording sequence showing maximum Z projection and single plane pictures of a transiently splitting (white arrow) *Math1::tdTomato-F*-positive dl1 growth cone (white arrowhead) in the FP with basal feet structures in between the two split branches (yellow arrowhead). SC, spinal cord; r, rostral; c, caudal; d, dorsal; v, ventral. Scale bars: 50 μ m (b-d), 25 μ m (e), and 10 μ m (f-l)

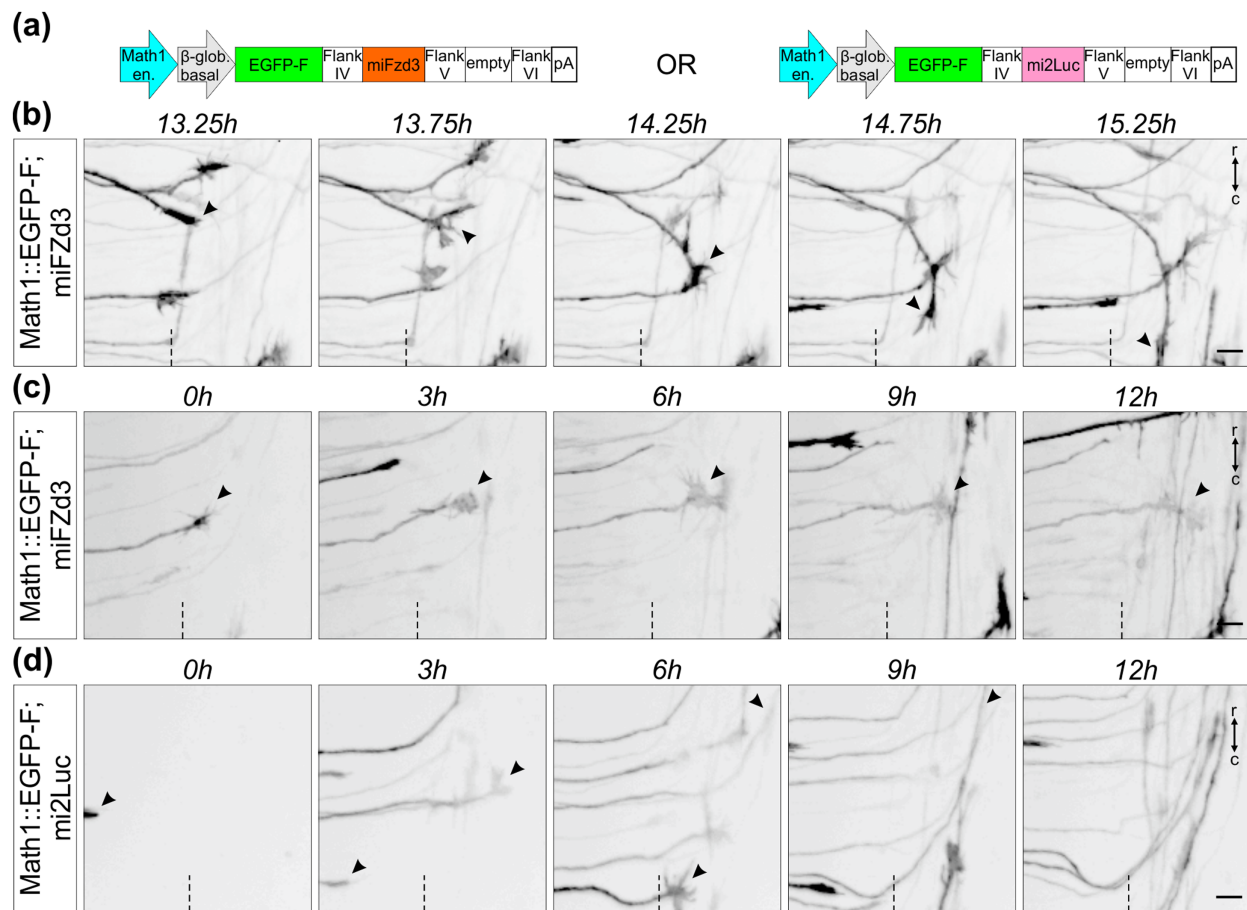


FIGURE 12 Live imaging after dl1 neuron-specific knockdown can be used to visualize mutant axons in intact spinal cord preparations. (a) Schematics depicting the plasmid constructs used to knockdown Fzd3 in dl1 neurons. A plasmid expressing a microRNA against luciferase (mi2Luc) was used as a control. (b) Time-lapse sequence showing a dl1 commissural axon turning caudally instead of rostrally at the contralateral floor plate (FP) border after silencing Fzd3 (black arrowheads). (c) Time-lapse sequence showing a dl1 commissural axon stalling at the contralateral FP border after silencing Fzd3 (black arrowheads). The growth cone kept remodeling but was not able to turn in either direction. (d) Time-lapse sequence showing dl1 axons expressing a microRNA against luciferase. These axons were not impacted and after exiting the FP they all turned rostrally (black arrowheads). Dashed black line represents the FP exit site. r, rostral; c, caudal. Scale bars: 10 μ m

the FP exit site without initiating any turn (black arrowhead, Figure 12 (c), Movie 25). Nonetheless, the growth cones remained highly dynamic. The changes in morphology were accompanied with transient retraction and re-extension but without a clear change in directionality. Importantly, expressing a control microRNA (mi2Luc) did not impact the guidance of dl1 axons at the contralateral FP border (Figure 12(d), Movie 26). Taken together, our method can be used to study the behavior of axons after perturbation of candidate genes specifically either in the neurons or in their target in real time, providing information about the dynamic behavior of growth cones and/or target cells that cannot be appreciated from snapshots taken from different preparations at selected time points.

4 | DISCUSSION

The possibility to follow one axon over time, rather than deducing behavior from snapshots of different axons, allowed us to extract

detailed information on the timing of midline crossing and the tight interaction between FP cells and the growth cones in a higher vertebrate model (Figure 13). Our ex vivo system offers significant improvement over existing open-book culture systems, as it not only allows for observation of growth cones within the midline area but also during and after their turn into the longitudinal axis. In cultures of open-book preparations, the deformation of the tissue, the lack of meninges that might restrict diffusion of secreted guidance cues, as seen for Shh, and the apoptosis in the ventral spinal cord could explain the guidance artifacts at the contralateral FP border (Figures 3–5) (Pignata et al., 2019). Our ex vivo culture system is highly reproducible and generates a manageable amount of data compared to live imaging using light sheet-based microscopy, for example (Liu et al., 2018).

The comparison of growth cones at the FP (this study) and at the optic chiasm (Godement et al., 1994; Sretavan & Reichardt, 1993) reveals both common and different behaviors. As seen at the chiasm (Godement et al., 1994), growth cones exhibited a saltatory growth behavior during FP crossing. However, in contrast to the chiasm, where

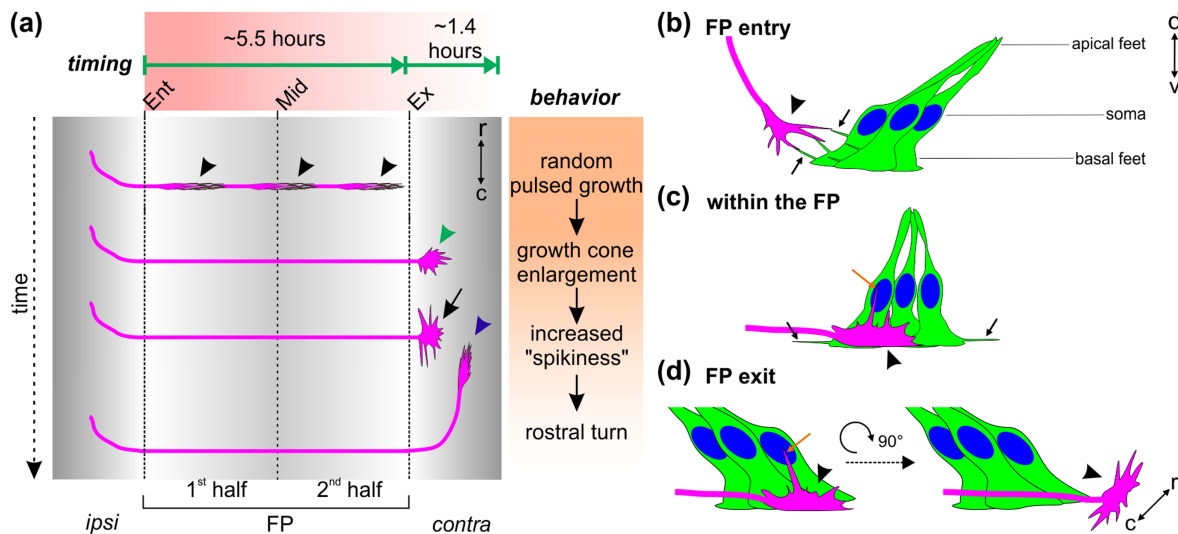


FIGURE 13 Cartoon depicting the midline crossing characteristics of dl1 axons based on data extracted from our ex vivo culture system. (a) On average, it took dl1 axons 5.6 h to cross the midline. Growth cones showed a random pulsed growth and had a thin shape in the growth direction (black arrowheads). At the floor plate (FP) exit site, dl1 growth cones were first enlarged (green arrowhead), then extended filopodia along the longitudinal axis (black arrow) right before turning rostrally (blue arrowhead). After arriving at the exit site of the FP, it took dl1 axons on average about 1.4 h to turn rostrally. In fact, the first-exiting dl1 axons took longer to turn rostrally than the late exiting ones. (b–d) Live imaging of intact spinal cords ex vivo using a high magnification objective shed light on dl1 growth cone orientation, FP morphology and dynamics during midline crossing. (b) While dl1 growth cones (black arrowhead) approached the FP, basal feet of lateral FP cells sent protrusions toward them and eventually interacted with them (black arrows). (c) When dl1 growth cones crossed the FP (black arrowhead), their dorso-ventral orientation aligned perfectly with the orientation of basal feet of medial FP cells. While basal feet of FP cells sent protrusions in axonal growth direction (black arrows), dl1 growth cones sent long filopodia in direction of the apical FP, toward the FP cell soma (orange arrow). (d) Just before exiting the FP, dl1 growth cones showed dorso-ventral activity with a long protrusion growing toward the FP soma (orange arrow) area followed by a 90° change in their orientation to become flattened in the dorso-ventral axis and enlarged in the longitudinal axis (black arrowhead). Ent, entry; Mid, midline; Ex, exit; r, rostral; c, caudal; ipsi, ipsilateral; contra, contralateral

axons would stall for several hours, axons did not pause during FP crossing. Growth speed in the FP was slower (5–75 $\mu\text{m}/\text{h}$) compared to that of retinal ganglion cell axons at the chiasm (60–100 $\mu\text{m}/\text{h}$). As described for the chiasm, growth cone morphology changed according to the dynamic behavior of the growth cone. During elongation of the axon, after entering the FP and before reaching the contralateral side, growth cones had a streamlined morphology. At the FP exit site, growth cone morphology changed to a much more complex shape with extended filopodia exploring the environment before the actual turn. At the chiasm, crossing axons did not change their morphology significantly, whereas those that changed their trajectory to turn along the ipsilateral pathway displayed a dramatic shape change just before the turn. Therefore, this resembles the behavior at the FP exit site, where a new direction is adopted by turning into the longitudinal axis.

Our comparative analyses demonstrate that midline crossing of dl1 axons in our ex vivo system was very similar to what happens in vivo (Figures 3–6). Therefore, our ex vivo system can be used to monitor and assess axonal behavior at choice points. We could detect that dl1 growth cones took on average 5.6 h to cross the entire FP and that they did so in a pulsed manner (black arrowheads, Figure 13). We could also measure that they needed on average 1.4 h to initiate their rostral growth, and that the first axons exiting the FP took longer than the followers (Figure 13(a)). In total they needed almost 7 h from entering the FP to making the decision to turn rostrally (blue

arrowhead, Figure 13(a)). This is enough time for growth cones to change their responsiveness to specific guidance cues for crossing and exiting the FP as well as for turning rostrally due to changes in receptor expression regulated at the posttranslational, translational, and even transcriptional level (Nawabi et al., 2010; Philipp et al., 2012; Pignata et al., 2019; Preitner et al., 2016; Stoeckli, 2018; Wilson & Stoeckli, 2013).

The growth cone is the decision center where axon guidance instructions are transduced to the cytoskeleton (Vitriol & Zheng, 2012). With our newly developed ex vivo system, dynamic changes in dl1 commissural growth cone morphology and behavior at the midline can be observed in real time. Growth cones were thin and elongated in the FP with their major extension in the dorso-ventral axis (black arrowheads, Figure 13(a,c)). At the FP exit site, they showed a 90° rotation to be enlarged and active in the longitudinal axis (green arrowhead and black arrow, Figure 13(a), black arrowhead, Figure 13(d)). The fact that dl1 growth cones sent a long filopodium into the FP, toward the FP cell soma area, while crossing it and just before exiting it, suggests that they might need to read signals from this area in order to move on and exit the FP (orange arrows in Figure 13(c,d)). The extension of long filopodia just before FP exit and rostral turning suggests that actin polymerization might be required to sense repulsive cues—for instance, SlitN and Shh, respectively—and transduce the signal into the growth cone, as suggested for

Slit-induced growth cone collapse in vitro (McConnell et al., 2016). Further investigations using our ex vivo culture system will be required to understand the role of cytoskeletal dynamics in axonal navigation of the intermediate target.

Our method also suggested a probable active contribution of FP cells to axon guidance that goes beyond providing axon guidance cues, as we found the cells of the intermediate target to be very dynamic and to extend protrusions in directions of the arriving axons, or to actively engage with axons in the FP. Thus, it seems that the intermediate target is much more than a passive by-stander and provider of attractive and repulsive axon guidance and cell adhesion molecules. We characterized the FP cell morphologies in detail in the medial as well as the lateral FP. Basal feet appeared to be enlarged and oriented parallel to commissural growth cones (Figure 13(c)). This was in line with previous reports in the chicken and mouse embryos (Campbell & Peterson, 1993; Ducuing et al., 2020; Yaginuma et al., 1991; Yoshioka & Tanaka, 1989). The lateral FP basal feet sent protrusions (black arrows) toward dl1 growth cones approaching the FP and eventually interacted with them (black arrowhead, Figure 13(b)). This intriguing observation led us to speculate whether these protrusions might be cytonemes. Cytonemes are long protrusions known to spread and deliver morphogens, such as Wnts and Shh, to neighboring or more distant cells (González-Méndez et al., 2019; Sanders et al., 2013; Stanganello & Scholpp, 2016). Given the fact that Shh is involved in guiding precrossing commissural axons toward the FP and that Shh and Wnts are both involved in guiding postcrossing axons toward the brain at the contralateral FP border, it is tempting to speculate that these protrusions might deliver such signals to the growth cones at choice points (Avilés et al., 2013). Moreover, we could appreciate how much the axons and their growth cones were intermingled within the medial FP basal feet which also formed long dynamic protrusions within the commissure (black arrowheads, Figure 13(c)). In sum, the combination of our live imaging approach with a FP-specific marker will give the opportunity to further characterize the behavior of intermediate target cells with regard to axon guidance at choice points.

Ultimately, our method will be useful to get more insights into molecular mechanisms of axon guidance at a choice point, when combined with in ovo RNAi for specific gene knockdowns either in the neurons or in their environment, as exemplified with Fzd3 knockdown experiments (Figure 12) (Andermatt et al., 2014; Baeriswyl et al., 2020; Pekarik et al., 2003). Similarly, pharmacological blockers will permit to screen for components required downstream of growth cone receptors to transduce guidance signals. Usually such experiments are conducted in vitro with cultured neurons growing axons in a very artificial environment. Thus, our method offers the advantages of an in vitro experiment in an intact complex “in vivo-like” environment. The use of specific reporters will also allow for the assessment of dynamic changes of second messengers or the actin cytoskeleton in growth cones, for example (Nichols & Smith, 2019; Nicol et al., 2011). Moreover, the use of other sets of enhancers and promoters might offer the possibility to study the dynamics of midline crossing in other subtypes of commissural neurons in the spinal cord and in the brain (Hadas et al., 2014; Kohl et al., 2012).

ACKNOWLEDGMENTS

The authors thank Dr Beat Kunz for excellent technical assistance. This project was supported by the Swiss National Science Foundation.

CONFLICT OF INTEREST

The authors declare no conflict of interests.

AUTHOR CONTRIBUTIONS

Alexandre Dumoulin: Designed experiments, performed experiments, evaluated data, and contributed to the writing of the manuscript.

Nikole R. Zuñiga: Generated the Hoxa1 plasmid. **Esther T. Stoeckli:** Designed experiments, supervised the project, and contributed to the writing of the manuscript.

PEER REVIEW

The peer review history for this article is available at <https://publons.com/publon/10.1002/cne.25107>.

DATA AVAILABILITY STATEMENT

The data that support the findings of this study are available from the corresponding author upon reasonable request.

ORCID

Alexandre Dumoulin  <https://orcid.org/0000-0002-2420-6877>

Nikole R. Zuñiga  <https://orcid.org/0000-0002-4022-9649>

Esther T. Stoeckli  <https://orcid.org/0000-0002-8485-0648>

REFERENCES

- Alther, T. A., Domanitskaya, E., & Stoeckli, E. T. (2016). Calsyntenin 1-mediated trafficking of axon guidance receptors regulates the switch in axonal responsiveness at a choice point. *Development (Cambridge)*, 143(6), 994–1004. <https://doi.org/10.1242/dev.127449>
- Andermatt, I., Wilson, N., & Stoeckli, E. T. (2014). In ovo electroporation of miRNA-based-plasmids to investigate gene function in the developing neural tube. *Methods in Molecular Biology*, 1101, 353–368. https://doi.org/10.1007/978-1-62703-721-1_17
- Avilés, E. C., Wilson, N. H., & Stoeckli, E. T. (2013). Sonic hedgehog and Wnt: Antagonists in morphogenesis but collaborators in axon guidance. *Frontiers in Cellular Neuroscience*, 7, 86. <https://doi.org/10.3389/fncel.2013.00086>
- Baeriswyl, T., Dumoulin, T., Schaettin, M., Tsapara, G., Niederkofler, V., Helbling, D., Avilés, E., Frei, J. A., Wilson, N.H., Gesemann, M., Kunz, B., & Stoeckli, E. T. (2020). Endoglycan plays a role in axon guidance and neuronal migration by negatively regulating cell-cell adhesion. *BioRxiv*, 425207. <https://doi.org/10.1101/425207>
- Boubakar, L., Falk, J., Ducuing, H., Thoinet, K., Reynaud, F., Derrington, E., & Castellani, V. (2017). Molecular memory of morphologies by septins during neuron generation allows early polarity inheritance. *Neuron*, 95(4), 834–851.e5. <https://doi.org/10.1016/j.neuron.2017.07.027>
- Bourikas, D., Pekarik, V., Baeriswyl, T., Grunditz, Å., Sadhu, R., Nardó, M., & Stoeckli, E. T. (2005). Sonic hedgehog guides commissural axons along the longitudinal axis of the spinal cord. *Nature Neuroscience*, 8(3), 297–304. <https://doi.org/10.1038/nn1396>
- Bovolenta, P., & Dodd, J. (1990). Guidance of commissural growth cones at the floor plate in embryonic rat spinal cord. *Development*, 109(2), 435–447.
- Burstyn-Cohen, T., Tzarfaty, V., Frumkin, A., Feinstein, Y., Stoeckli, E., & Klar, A. (1999). F-spondin is required for accurate pathfinding of

- commissural axons at the floor plate. *Neuron*, 23(2), 233–246. [https://doi.org/10.1016/S0896-6273\(00\)80776-X](https://doi.org/10.1016/S0896-6273(00)80776-X)
- Campbell, R. M., & Peterson, A. C. (1993). Expression of a lacZ transgene reveals floor plate cell morphology and macromolecular transfer to commissural axons. *Development*, 119(4), 1217–1228.
- Das, R. M., & Storey, K. G. (2014). Apical abscission alters cell polarity and dismantles the primary cilium during neurogenesis. *Science*, 343(6167), 200–204. <https://doi.org/10.1126/science.1247521>
- de Ramon Francàs, G., Zuñiga, N. R., & Stoeckli, E. T. (2017). The spinal cord shows the way—How axons navigate intermediate targets. *Developmental Biology*, 432, 43–52. <https://doi.org/10.1016/j.ydbio.2016.2.002>
- Domanitskaya, E., Wacker, A., Mauti, O., Baeriswyl, T., Esteve, P., Bovolenta, P., & Stoeckli, E. T. (2010). Sonic hedgehog guides post-crossing commissural axons both directly and indirectly by regulating Wnt activity. *Journal of Neuroscience*, 30(33), 11167–11176. <https://doi.org/10.1523/JNEUROSCI.1488-10.2010>
- Ducuing, H., Gardette, T., Pignata, A., Kindbeiter, K., Bozon, M., Thoumine, O., Delloye-Bourgeois, C., Tauszig-Delamasure, S., & Castellani, V. (2020). SlitC-PlexinA1 mediates iterative inhibition for orderly passage of spinal commissural axons through the floor plate. *eLife*, 9, e63205. <https://doi.org/10.7554/eLife.63205>
- Dumoulin, A., Dagane, A., Dittmar, G., & Rathjen, F. G. (2018). S-palmitoylation is required for the control of growth cone morphology of DRG neurons by CNP-induced cGMP signaling. *Frontiers in Molecular Neuroscience*, 11, 345. <https://doi.org/10.3389/fnmol.2018.00345>
- Fitzli, D., Stoeckli, E. T., Kunz, S., Siribour, K., Rader, C., Kunz, B., Kozlov, S. V., Buchstaller, A., Lane, R. P., Suter, D. M., Dreyer, W. J., & Sonderegger, P. (2000). A direct interaction of axonin-1 with NgCAM-related cell adhesion molecule (NrcAM) results in guidance, but not growth of commissural axons. *Journal of Cell Biology*, 149(4), 951–968. <https://doi.org/10.1083/jcb.149.4.951>
- Godement, P., Wang, L. C., & Mason, C. A. (1994). Retinal axon divergence in the optic chiasm: Dynamics of growth cone behavior at the midline. *Journal of Neuroscience*, 14(11 II), 7024–7039. <https://doi.org/10.1523/jneurosci.14-11-07024.1994>
- González-Méndez, L., Gradilla, A. C., & Guerrero, I. (2019). The cytoneme connection: Direct long-distance signal transfer during development. *Development (Cambridge)*, 146(9), dev174607. <https://doi.org/10.1242/dev.174607>
- Hadas, Y., Etlin, A., Falk, H., Avraham, O., Kobiler, O., Panet, A., Lev-Tov, A., & Klar, A. (2014). A “tool box” for deciphering neuronal circuits in the developing chick spinal cord. *Nucleic Acids Research*, 42(19), e148. <https://doi.org/10.1093/nar/gku750>
- Hamburger, V., & Hamilton, H. L. (1951). A series of normal stages in the development of the chicken embryo. *Journal of Morphology*, 88, 49–92.
- Kohl, A., Hadas, Y., Klar, A., & Sela-Donenfeld, D. (2012). Axonal patterns and targets of dA1 interneurons in the chick hindbrain. *Journal of Neuroscience*, 32(17), 5757–5771. <https://doi.org/10.1523/jneurosci.4231-11.2012>
- Li, X., & Lufkin, T. (2000). Cre recombinase expression in the floorplate, notochord and gut epithelium in transgenic embryos driven by the Hoxa-1 enhancer III. *Genesis*, 26(2), 121–122. [https://doi.org/10.1002/\(SICI\)1526-968X\(200002\)26:2<121::AID-GENE6>3.0.CO;2-T](https://doi.org/10.1002/(SICI)1526-968X(200002)26:2<121::AID-GENE6>3.0.CO;2-T)
- Li, Y., Vieceli, F. M., Gonzalez, W. G., Li, A., Tang, W., Lois, C., & Bronner, M. E. (2019). In vivo quantitative imaging provides insights into trunk neural crest migration. *Cell Reports*, 26(6), 1489–1500.e3. <https://doi.org/10.1016/j.celrep.2019.01.039>
- Liu, T. L., Upadhyayula, S., Milkie, D. E., Singh, V., Wang, K., Swinburne, I. A., Mosaliganti, K. R., Collins, Z. M., Hiscock, T. W., Shea, J., Kohrman, A. Q., Medwig, T. N., Dambournet, D., Forster, R., Cunniff, B., Ruan, Y., Yashiro, H., Scholpp, S., Meyerowitz, E. M., ... Betzig, E. (2018). Observing the cell in its native state: Imaging subcellular dynamics in multicellular organisms. *Science*, 360(6386), eaaq1392. <https://doi.org/10.1126/science.aaq1392>
- Long, H., Sabatier, C., Ma, L., Plump, A., Yuan, W., Ornitz, D. M., ... Tessier-Lavigne, M. (2004). Conserved roles for Slit and Robo proteins in midline commissural axon guidance. *Neuron*, 42(2), 213–223. [https://doi.org/10.1016/S0896-6273\(04\)00179-5](https://doi.org/10.1016/S0896-6273(04)00179-5)
- Lyuksytova, A. I., Lu, C. C., Milanesio, N., King, L. A., Guo, N., Wang, Y., Nathans, J., Tessier-Lavigne, M., & Zou, Y. (2003). Anterior-posterior guidance of commissural axons by Wnt-frizzled signaling. *Science*, 302(5652), 1984–1988. <https://doi.org/10.1126/science.1089610>
- McConnell, R. E., van Veen, J. E., Vidaki, M., Kwiatkowski, A. V., Meyer, A. S., & Gertler, F. B. (2016). A requirement for filopodia extension toward Slit during Robo-mediated axon repulsion. *Journal of Cell Biology*, 213(2), 261–274. <https://doi.org/10.1083/jcb.201509062>
- Medioni, C., Ephrussi, A., & Besse, F. (2015). Live imaging of axonal transport in Drosophila pupal brain explants. *Nature Protocols*, 10(4), 574–584. <https://doi.org/10.1038/nprot.2015.034>
- Meijering, E., Dzyubachyk, O., & Smal, I. (2012). Methods for cell and particle tracking. In *Methods in enzymology* (Vol. 504, pp. 183–200). Elsevier. <https://doi.org/10.1016/B978-0-12-391857-4.00009-4>
- Nawabi, H., Briancçon-Marjollet, A., Clark, C., Sanyas, I., Takamatsu, H., Okuno, T., ... Castellani, V. (2010). A midline switch of receptor processing regulates commissural axon guidance in vertebrates. *Genes and Development*, 24(4), 396–410. <https://doi.org/10.1101/gad.542510>
- Nichols, E. L., & Smith, C. J. (2019). Pioneer axons employ Cajal's battering ram to enter the spinal cord. *Nature Communications*, 10(1), 562. <https://doi.org/10.1038/s41467-019-08421-9>
- Nicol, X., Hong, K. P., & Spitzer, N. C. (2011). Spatial and temporal second messenger codes for growth cone turning. *Proceedings of the National Academy of Sciences of the United States of America*, 108(33), 13776–13781. <https://doi.org/10.1073/pnas.1100247108>
- Pekarik, V., Bourikas, D., Miglino, N., Joset, P., Preiswerk, S., & Stoeckli, E. T. (2003). Screening for gene function in chicken embryo using RNAi and electroporation. *Nature Biotechnology*, 21(1), 93–96. <https://doi.org/10.1038/nbt770>
- Phan, K. D., Hazen, V. M., Frenzo, M., Jia, Z., & Butler, S. J. (2010). The bone morphogenetic protein roof plate chemorepellent regulates the rate of commissural axonal growth. *Journal of Neuroscience*, 30(46), 15430–15440. <https://doi.org/10.1523/JNEUROSCI.4117-10.2010>
- Philipp, M., Niederkofler, V., Debrunner, M., Alther, T., Kunz, B., & Stoeckli, E. T. (2012). RabGDI controls axonal midline crossing by regulating Robo1 surface expression. *Neural Development*, 7(1), 36. <https://doi.org/10.1186/1749-8104-7-36>
- Pignata, A., Ducuing, H., Boubakar, L., Gardette, T., Kindbeiter, K., Bozon, M., Tauszig-Delamasure, S., Falk, J., Thoumine, O., & Castellani, V. (2019). A spatiotemporal sequence of sensitization to slits and semaphorins orchestrates commissural axon navigation. *Cell Reports*, 29(2), 347–362.e5. <https://doi.org/10.1016/j.celrep.2019.08.098>
- Preitner, N., Quan, J., Li, X., Nielsen, F. C., & Flanagan, J. G. (2016). IMP2 axonal localization, RNA interactome, and function in the development of axon trajectories. *Development (Cambridge)*, 143(15), 2753–2759. <https://doi.org/10.1242/dev.128348>
- Sanders, T. A., Llagostera, E., & Barna, M. (2013). Specialized filopodia direct long-range transport of SHH during vertebrate tissue patterning. *Nature*, 497(7451), 628–632. <https://doi.org/10.1038/nature12157>
- Schindelin, J., Arganda-Carreras, I., Frise, E., Kaynig, V., Longair, M., Pietzsch, T., Preibisch, S., Rueden, C., Saalfeld, S., Schmid, B., Tinevez, J. Y., White, D. J., Hartenstein, V., Eliceiri, K., Tomancak, P., & Cardona, A. (2012). Fiji: An open-source platform for biological-image analysis. *Nature Methods*, 9, 676–682. <https://doi.org/10.1038/nmeth.2019>

- Siegenthaler, J. A., & Pleasure, S. J. (2011). We have got you "covered": How the meninges control brain development. *Current Opinion in Genetics and Development*, 21, 249–255. <https://doi.org/10.1016/j.gde.2010.12.005>
- Sretavan, D. W., & Reichardt, L. F. (1993). Time-lapse video analysis of retinal ganglion cell axon pathfinding at the mammalian optic chiasm: Growth cone guidance using intrinsic chiasm cues. *Neuron*, 10(4), 761–777. [https://doi.org/10.1016/0896-6273\(93\)90176-R](https://doi.org/10.1016/0896-6273(93)90176-R)
- Stanganello, E., & Scholpp, S. (2016). Role of cytonemes in Wnt transport. *Journal of Cell Science*, 129(4), 665–672. <https://doi.org/10.1242/jcs.182469>
- Stoeckli, E. T. (2018). Understanding axon guidance: Are we nearly there yet? *Development (Cambridge)*, 145, dev151415. <https://doi.org/10.1242/dev.151415>
- Stoeckli, E. T., & Landmesser, L. T. (1995). Axonin-1, nr-CAM, and Ng-CAM play different roles in the in vivo guidance of chick commissural neurons. *Neuron*, 14(6), 1165–1179. [https://doi.org/10.1016/0896-6273\(95\)90264-3](https://doi.org/10.1016/0896-6273(95)90264-3)
- Vitriol, E. A., & Zheng, J. Q. (2012). Growth cone travel in space and time: The cellular ensemble of cytoskeleton, adhesion, and membrane. *Neuron*, 73, 1068–1081. <https://doi.org/10.1016/j.neuron.2012.03.005>
- Wilson, N. H., & Stoeckli, E. T. (2011). Cell type specific, traceable gene silencing for functional gene analysis during vertebrate neural development. *Nucleic Acids Research*, 39(20), e133. <https://doi.org/10.1093/nar/gkr628>
- Wilson, N. H., & Stoeckli, E. T. (2012). In ovo electroporation of miRNA-based plasmids in the developing neural tube and assessment of phenotypes by Dil injection in open-book preparations. *Journal of Visualized Experiments*, 68, 4384. <https://doi.org/10.3791/4384>
- Wilson, N. H., & Stoeckli, E. T. (2013). Sonic hedgehog regulates its own receptor on postcrossing commissural axons in a glypican1-dependent manner. *Neuron*, 79(3), 478–491. <https://doi.org/10.1016/j.neuron.2013.05.025>
- Wright, K. M., Lyon, K. A., Leung, H., Leahy, D. J., Ma, L., & Ginty, D. D. (2012). Dystroglycan organizes axon guidance Cue localization and axonal pathfinding. *Neuron*, 76(5), 931–944. <https://doi.org/10.1016/j.neuron.2012.10.009>
- Yaginuma, H., Homma, S., Künzi, R., & Oppenheim, R. W. (1991). Pathfinding by growth cones of commissural interneurons in the chick embryo spinal cord: A light and electron microscopic study. *Journal of Comparative Neurology*, 304(1), 78–102. <https://doi.org/10.1002/cne.903040107>
- Yoshioka, T., & Tanaka, O. (1989). Ultrastructural and cytochemical characterisation of the floor plate ependyma of the developing rat spinal cord. *Journal of Anatomy*, 165, 87–100.
- Zisman, S., Marom, K., Avraham, O., Rinsky-Halivni, L., Gai, U., Kligun, G., Tzarfaty-Majar, V., Suzuki, T., & Klar, A. (2007). Proteolysis and membrane capture of F-spondin generates combinatorial guidance cues from a single molecule. *Journal of Cell Biology*, 178(7), 1237–1249. <https://doi.org/10.1083/jcb.200702184>
- Zou, Y. (2012). Does planar cell polarity signaling steer growth cones? *Current Topics in Developmental Biology*, 101, 141–160. <https://doi.org/10.1016/B978-0-12-394592-1.00009-0>

SUPPORTING INFORMATION

Additional supporting information may be found online in the Supporting Information section at the end of this article.

How to cite this article: Dumoulin A, Zuñiga NR, Stoeckli ET. Axon guidance at the spinal cord midline—A live imaging perspective. *J Comp Neurol*. 2021;529:2517–2538. <https://doi.org/10.1002/cne.25107>